Borehole Investigations of Firn Processes

Robert L. Hawley

A dissertation submitted in partial fulfillment
of the requirements for the degree of

Doctor of Philosophy

University of Washington

2005

Program Authorized to Offer Degree: Department of Earth and Space Sciences -
Geophysics

ProQuest Information and Learning Company
300 North Zeeb Road
P.O. Box 1346
Ann Arbor, MI 48106-1346

University of Washington
Graduate School

This is to certify that I have examined this copy of a doctoral dissertation by

Robert L. Hawley

and have found that it is complete and satisfactory in all respects,
and that any and all revisions required by the final
examining committee have been made.

Chair of Supervisory Committee:

Edwin D. Waddington

Edwin D. Waddington

Reading Committee:

Edwin D. Waddington

Edwin D. Waddington

Dale P. Winebrenner

Dale P. Winebrenner

Stephen G. Warren.

Stephen G. Warren

Date: 18 Feb 2005

Signature

Date 24 Feb 2005

University of Washington

Abstract

Borehole Investigations of Firn Processes

by Robert L. Hawley

Chair of Supervisory Committee:

Professor Edwin D. Waddington
Department of Earth and Space Sciences

Information on paleoclimate and firn processes can be obtained from the shallow regions of an ice sheet via borehole logging. I introduce a method for measuring vertical strain in a borehole using a borehole video camera and artificial marking bands. The method uses image processing to determine the distance from the camera to a marker. One product of these measurements is a depth-age scale for the firn at Taylor Dome. The age of an ash layer in the core is 675 ± 25 years. I compare this method with a similar method using a metal detector to locate the markers. Data collected at Siple Dome with the two methods agrees, and I discuss the merits of each system. From a similar analysis to that used for Taylor Dome, the same ash layer found in both cores has an age of 665 ± 30 years at Siple Dome, in agreement with the measurements from Taylor Dome. I develop a method for measuring vertical motion using natural markers in the borehole wall. This method determines the returned brightness from an annular region of the borehole wall, and produces a Borehole Optical Stratigraphic (BOS) profile. Features in this BOS profile can be tracked to determine strain. Using data from Summit, Greenland, I calculate the vertical strain that took place between 2 logs taken 70 days apart. Annual layers can be resolved in the BOS signal. A depth-age scale for the firn at Siple Dome, made by counting these annual layers, agrees with similar depth-age scales produced by traditional stratigraphy on the core. I investigate the relationship between the BOS signal and the detailed firn density

profile provided by the Wallingford Neutron Scattering density probe. The BOS and density profiles show positive correlation near the surface, with correlation decreasing and becoming negative near the bottom of the survey at 30 meters. This phenomenon could be related to the transitions between densification-mechanism regimes.

TABLE OF CONTENTS

LIST OF FIGURES

Figure Number Page

LIST OF TABLES

ACKNOWLEDGMENTS

While a dissertation is the culmination of one person's graduate school education and there is only one name on the front, nobody can do good science in a vacuum, and I have benefited from the assistance of countless individuals over my time at the University of Washington, and to list them all here would be an impossible task. Since this issue has generally not stopped me before, however, I list below some of the most important- if I have left you off the list I apologize.

First and foremost, the experience of a graduate student is shaped by the advisor, and I have been fortunate to be advised by Ed Waddington. He has been an excellent advisor and collaborator, in all aspects of science and also in our public outreach efforts, and I look forward to collaborating more in the future.

I wold also like to thank the rest of my advisory committee, Charlie Raymond, Dale Winebrenner, and Steve Warren, for the help and guidance they have given me over the years. Howard Conway deserves special mention here as well, for although not officially a member of my committee, he has given me much help and advice.

The graduate students in the glaciology group have been great to work with. Tom Neumann in particular has helped me in all stages of my graduate career, from helping me retrain myself in differential equations to giving advice on negotiating job offers, and has been a good friend. It is said that if you want to train to run a marathon it's helpful to have a training partner, and I've been glad to have Ginny Catania to traverse the same courses and dissertation pitfalls with. Having been in the same office for as long as I have, I've had a slew of excellent office mates, including H-P. Marshall, Al Rasmussen, Tim Schaub, Paul Jacobsen, Throstur Thorsteinsson, Kurt Cuffey, Shannon McDaniel, Steve Price, Lars Karlof, Michelle Koutnik, and Joe MacGregor. In addition, I've benefited from the help of my non-office-mate fellow graduate students Tony Gades, Nadine Nereson, Erin Pettit, and

Ben Smith.

Outside the University, I've had many great collaborations with researchers from other institutions. Gary Clow has been a great friend and partner in crime, and helped me get started in this business in the first place. In my field work I've had many fruitful discussions with Gregg Lamorey and Ryan Bay while endlessly logging deep boreholes in the cold wee hours of the morning.

Since several of my chapters have been published in journals, I'd like to thank the referees of these papers, who include Jacques Meyssonnier, Martin Funk, Tad Pfeffer, and Gordon Hamilton. In addition, I thank my co-authors on these chapters, Dave Morse, Richard Alley, Gregg Lamorey, Ken Taylor, Nelia Dunbar, Greg Zielinski, Liz Morris.

We all need to be better about bringing our research to the public, and Rolf Tremblay has been instrumental in helping me do this, through the Teachers Experiencing Antarctica program. Thanks also go to Sandra Kolb who helped Ed and me start our evening lecture career.

Most polar science cannot survive without funding, and mine is no exception. The work represented by this dissertation has been funded by National Science Foundation grants OPP-9221261, OPP-9421644, OPP-9526420, OPP-9726078, OPP-0087521, OPP-0087160, OPP-0126187, OPP-0335330, and OPP-0352584. Density data for chapter 6 was gathered with support from the UK Natural Environmental Research Council under grant NER/O/S/2003/00620. Parts of chapter 2 were funded by a Research Training Grant from the Mary Gates Foundation.

Even with good funding, polar field work could not succeed without good logistical support. I thank NSF contractors Antarctic Support Associates, Raytheon Polar Services, VECO polar resources (in particular Robin Abbott, Kathy Young, Paula Adkins, Meg Flanagan, Katie Hess, and Toby Wood), and Geoff Somers for support in the field. Chapter 4 was completed in part with the support of the Center for Advanced Research Technology in the Arts and Humanities (CARTAH) at the University of Washington. Boreholes are needed for borehole logging, and I thank the Polar Ice Coring Office and Ice Core Drilling

Services, and "leathery drillers" Jay Kyne and Beth Bergeron.

A student needs to exist outside the University world as well, and I'd like to thank the good friends who have helped make my life in Seattle full and happy. In particular I'd like to single out Brian Peterka, who perhaps unwittingly helped set me on the path that has brought me here by opening my eyes to the possibility of working in the Antarctic.

I thank my family, immediate and extended, for all the unconditional love and support they have given me. In particular, I thank my father for helping me learn over the years many skills and values that have served me very well throughout all aspects of my life, and particularly in polar science.

Finally and most importantly, I thank my wife Suzanne who has had immense patience, given me unflagging love and support, helped me keep perspective, kept me sane, given me good advice, and given up countless weekends as I negotiated graduate school. Without her this process would not have been possible. I look forward eagerly to our next adventure, as we continue down this path together.

DEDICATION

To my dad
who has taught me more than anyone.

And in memory of my mom
who showed me how to be of use.

Chapter 1

INTRODUCTION

1.1 Motivation and Background

> The climate system is an angry beast and we are poking it with sticks.
>
> – Wallace Broecker

Global climate change is an important issue today. The Intergovernmental Panel on Climate Change has stated that increased temperatures and precipitation in the coming decades may lead to decreased crop yields, increased energy demand, and increased frequency and intensity of tropical cyclones, among other things (Houghton and others, 2001). In the last hundred years the world's anthropogenic output of greenhouse gases has increased to a level never before seen. It is clear that humans have had an impact on the climate in the last hundred years. Yet the makers of government policy demand "proof-positive" that the changes we make are detrimental. The climate system is a complex one, subject to the effects of many interconnected variables. One way to determine if the changes we make are detrimental is to make the changes and see if we adversely affect the climate system. This is probably not a good approach, since this is a system we know little about and it leaves the earth as the only "canary in the coal mine"; once we can see the damage it may well be too late to take corrective action.

In order to predict what the climate system will do in the future, we need to understand 2 important issues: 1) the climate changes of the past- what was it doing then?, and 2) the current state of the climate system- what is it doing now?

1.1.1 Paleoclimate

Although any financial advisor will tell you that past performance is no guarantee of future results, often the best instrument we have for inspecting how the climate changes in time is a study of past climate. Paleoclimatology draws on many different records to piece together the puzzle of what climate was like in the past. From the oceans where sediment continuously rains out of the sea, sediment cores contain tracers that are clues. Short temporal records can be obtained from tree rings. For a relatively long record with good resolution, many scientists turn to ice cores. In the layers of ice that are stacked one on top of the other, ice cores retain records of temperature and precipitation, along with traces of chemicals that might have affected the atmosphere.

Although an ice core preserves temporal detail in the climate record, spatially it is a point measurement. Since an ice core is expensive and time consuming to drill, the location must be chosen with care. Borehole studies can assist in the site-selection process by determining vertical motion as part of an ice-dynamics study and by determining the depth-age relationship at a site. This depth-age scale can be determined quickly from a borehole log. The speed with which we can make these measurements can also allow us to extend our reach beyond the local area of a core, and begin to do stratigraphic studies over a larger region.

1.1.2 Current climate

In addition to studying past climate, we need to understand what the climate system is doing presently. Glaciers and ice sheets are a good way of looking for changes that occur over long time scales- they advance and retreat with climate changes.

The measurement of mass balance, mass gained or lost by a glacier in a given period, is probably one of the oldest ways to study the "health" of a glacier or ice sheet. Modern methods of measuring the rise and fall of the surface of an ice sheet often involve remote sensing of the surface height from aircraft or spacecraft. The change in surface height over time dH/dt of an ice sheet is affected by many factors. These factors include snow accumulation at the surface $A(t)$, variations in the rate of firn compaction $v_{fc}(t)$ near the surface, ice dynamics $v_i(t)$, isostatic rebound of the underlying bedrock $b(t)$, and melting of ice at the bed $m(t)$:

$$\frac{dH}{dt} = A(t) - v_{fc}(t) - v_i(t) + b(t) - m(t) \tag{1.1}$$

Of these factors, $A(t)$ and $v_{fc}(t)$ are the largest terms in equation 1.1. Many studies have modeled firn densification through the years, with increasing realism and complexity. Recent studies have modeled the seasonal variations of firn densification, based on the temperature-dependence of the physical processes that drive densification.

While the modeling of firn densification has improved greatly in recent years, direct observations of densification or any kind of vertical motion in the field are rare. The density profile in a core can be studied, but this provides only a "snapshot" of a moment in time, and thus can at best provide a steady-state picture. A complete understanding of the time-dependent and seasonal nature of firn densification therefore requires field measurements. Borehole methods allow us to measure the actual motion of the firn.

1.1.3 Firn

Glacier ice was once snow that fell on the glacier or ice sheet. As it was buried under more snow, the snow became denser and denser until it became ice. From the time it fell on the surface of the ice sheet until the time it became ice, it underwent many changes. During this time it is called firn.

The term firn was defined for temperate glaciers, where it refers to snow in a glacial environment that has survived at least one melt season. On polar ice sheets, where there may never be any melt, the transition from "snow" to "firn" is undefined, and it is often common to neglect "snow" and refer to the entire upper several tens of meters as firn, from the surface to the depth at which pores close off, referred to as the "pore close-off depth" or the "firn-ice transition". Throughout this dissertation I have adhered to this definition.

The firn region of a polar ice sheet is an active one. Firn undergoes large changes as it becomes glacial ice. The most obvious change is densification, and indeed it is density that we commonly use to refer to a particular part of the firn, rather than depth, since density profiles vary according to climate. Other properties of ice crystals change in the firn as well. Ice grains metamorphose and change size. Crystal fabric may begin to develop. Firn also undergoes changes in chemistry as species are deposited or removed by air traveling through the firn, and some chemical species also diffuse through the firn. Aerosols from the atmosphere are trapped in the firn and gas from the atmosphere is sealed off as an archive when firn pores close.

In short, the firn is where ice cores get many of their interesting characteristics. Yet the firn is an under-studied part of the cryosphere.

1.1.4 Borehole logging

In this dissertation, I address firn processes from several different angles. All of these approaches are based upon in-situ measurements made possible by borehole logging. Borehole logging was pioneered as a geophysical field method in the early 1900's by brothers Marcel and Conrad Schlumberger. The technique consists of lowering a probe into a borehole to measure properties of the surrounding medium. Commonly used in the oil exploration industry today, borehole logging can provide information about structures deep within the earth or an ice sheet, and takes many forms, depending on the probe used. In this dissertation, I use information gathered mainly from borehole video logging, using post-processing image-analysis to quantify changes we can usually, but not always, see visually.

1.2 Organization of the dissertation

Each chapter in this dissertation is written as a stand-alone manuscript. Chapters 2 and 5 are in print in the *Journal of Glaciology* and *Geophysical Research Letters* respectively, Chapter 3 is in press at the *Journal of Glaciology*, and chapters 4 and 6 are in preparation for submission to the *Journal of Glaciology.* As these are individual stand-alone manuscripts, there is some overlap between some chapters, in text and to a lesser extent in the figures.

1.3 Synopsis

Chapters 2 through 4 are centered around measuring vertical strain in the firn, and what we can learn from these measurements. In chapter 2, I introduce a novel method for measuring vertical strain in polar firn using a borehole video camera and metal markers, and I derive a depth-age scale for the firn at Taylor Dome, Antarctica, using this method. Chapter 2 also uses the statistical technique of Bootstrapping, which has heretofore seen little use in glaciology. Chapter 3 compares this video method with another method for measuring vertical strain, which uses a resonating tuned coil to locate metal marking bands. In chapter 4, I develop a new method for measuring vertical strain in polar firn, again using a video camera but now eliminating the need for metal markers. Instead I use natural changes in the reflectivity of the borehole wall as markers.

Chapters 5 and 6 discuss additional information beyond vertical strain that can be learned by processing optical logs of polar firn. In chapter 5, I show that annual layers in the borehole wall can be resolved and counted to provide a depth-age profile of a borehole, and also to assist in deriving an accumulation history. In chapter 6, I use side-by-side detailed logs of optical brightness and density (as measured by the Wallingford neutron probe) to show that in the shallow regions the optical signal is strongly affected by density, and that deeper, the relationship between the optical signal and density changes.

Chapter 7 presents general conclusions, and suggests future directions for this line of research.

Chapter 2

DATING FIRN CORES BY VERTICAL STRAIN MEASUREMENTS

This chapter was published under the same title in *Journal of Glaciology* **48**(162) with co-authors Edwin D. Waddington, David L. Morse, Nelia W. Dunbar, and Gregory A. Zielinski. Helpful review comments were made by Jacques Meyssonnier, Martin Funk and Tad Pfeffer. The specific contributions of my co-authors were: Ed Waddington initiated the project to measure vertical strain, helped guide my research, and edited the manuscript. Dave Morse developed the conceptual idea of using a video camera to locate the markers. Nelia Dunbar and Greg Zielenski measured the ash in the Siple and Taylor Dome ice cores, and authored a paragraph in the manuscript regarding the ash.

2.1 Summary

We have developed a system for measuring a vertical strain rate profile in the firn on polar ice sheets using a readily available video camera to detect metal bands inserted in an air-filled hole. We used this system in 1995 and 1996 at Taylor Dome, Antarctica. We use density measurements combined with our strain rates to infer vertical velocities. From our velocities we calculate a steady state depth-age scale for the firn at Taylor Dome. The age of a visible ash layer from 79.1 meters is 675 ± 25 years; this ash can be correlated with ash found at 97.2 meters in a recent ice core at Siple Dome, West Antarctica.

2.2 Introduction

Firn cores can often be dated by counting annual horizons identified by geochemical analysis. It is useful, however, to have a physically based method of dating these same cores to confirm the geochemical ages, and to resolve any ambiguity in the geochemical interpretation where annual cycles in the chemistry may be poor or nonexistent. Where both geochemical and geophysical depth-age relationships exist, they can be compared to extract information on variations in accumulation rate. A physically based model can be derived from a measurement of the rate of vertical compaction in the firn. This measurement is also useful for heat and ice flow models.

Making such a measurement is not as straightforward as measuring horizontal motion at the surface, due to problems of access. We have developed a simple method to make this measurement using readily available hardware and software. We track markers placed at intervals in an existing borehole. Unlike previous methods that used a custom-built tuned coil detector to locate markers, we use a commercially available video camera.

2.3 Taylor Dome

Taylor Dome is an ice dome west of the Transantarctic mountains on the polar plateau of East Antarctica. First noted by Drewry (1982) in an aerial radio echo sounding survey of the area, it is centered at 77°50′S and 159°00′E, and is the source of ice for Taylor Glacier in the McMurdo Dry Valleys. It is the site of a 554 m ice core to bedrock, taken in the 1993-94 austral summer field season (Grootes and others, 1994; Fitzpatrick, 1994; Steig and others, 2000; Grootes and others, 2001). The recovered core contains a record of past climate in its isotopic, chemical, physical, and bubble gas properties. In order to interpret the core correctly, studies of the ice dynamics in the region of the drill site were carried out, starting in 1990 (Waddington and others, 1991; Grootes and others, 1991; Morse and Waddington, 1992; Waddington and others, 1993; Morse and Waddington, 1993; Waddington and others, 1994). A network of over 250 survey poles on the dome was surveyed repeatedly using optical, geoceiver (Transit Satellite), and Global Positioning System (GPS) methods. This network, which was also tied into bedrock points near Taylor Dome and a well-constrained point at McMurdo station, provides horizontal velocity and strain rates on the ice surface (Morse, 1997).

In an effort to further understand the bed topography and the internal structure of the ice in this region, extensive surface-based radio echo sounding surveys have been made (Morse and Waddington, 1993; Morse, 1997; Morse and others, 1998). These profiles provide accurate bed topography for flow modeling, and also show the internal layering of the ice. Other geochemical and physical studies have been done using the recovered core (Grootes and others, 1994). Three other cores were drilled, varying from 100 to 150 m in depth. One of these holes provided the opportunity to measure vertical motion.

2.4 Measurements

For our measurements, we used a 130 m deep, 15 cm diameter dry borehole located 50 m from the main hole at Taylor Dome. We placed markers in the hole at approximately 5 m intervals. Each marker is a 10 cm by 1 m strip of sheet phosphor bronze, coiled into a cylinder and released into the hole, where it expands to the size of the hole and holds to the wall by spring tension. A logging tool can pass through these markers. The custom tool used for injecting the bands was built by Phil Taylor of Hydro-Tech, based on the recommendations of Raymond and others (1994). Metal bands provide both a sharp edge contrast for video, and a conductive ring geometry that can be exploited by the tuned coil detection system developed by Rogers and LaChapelle (1974), and used at Dyer Plateau by Raymond and others (1996).

2.4.1 Instrument

Our video logging tool is a downward looking wide-angle video camera with integral Light Emitting Diodes (LEDs) to provide illumination. This charge-coupled device (CCD) camera is a "See Snake" model made by DeepSea Power & Light Inc. We mounted the camera in a simple rigid frame of about 10 cm diameter with tapered ends. We recorded images from the SeeSnake camera with an 8mm video camcorder.

The tool hangs by a single triaxial cable containing both video and power conductors. We also used the cable to measure the depth of the camera. We ran the cable over a pulley placed atop a survey tripod positioned over the hole. We raised and lowered the tool by hand. A camming cable brake attached to the pulley housing allowed the tool to hang suspended during measurements.

Once the bands were in place, we recorded their relative positions with the video logging tool in January 1995. One year later we repeated the survey. For the first log, we made a permanent mark on the cable when we could image each band. We measured the distance between this mark and the borehole casing with a vernier caliper (see Figure 2.1) for this and all subsequent images of this particular band edge.

The two dimensional image of a band in the hole (Figure 2.2) shows the edge of the band as a circle. We determine the location of the camera relative to the band by measuring the observed apparent radius of the band at a given camera position. The distance d between the camera lens and the edge of the band can be expressed in terms of the focal length f of the lens, the actual radius of the band r_a,and the observed radius of the band r_o:

$$d = \frac{f r_a}{r_o}. \tag{2.1}$$

Ideally we would select an optimum distance from each band to position the camera for caliper measurements, calculate the desired apparent radius r_d for that distance, and make the caliper measurement when the camera is positioned so that $r_o = r_d$. Since we did not have fine adjustment ability to position our tool, and had no accurate means of assessing the apparent radius in the field, we used the following "bracketing" approach to ensure we had positioned the camera in the same way from year to year.

For each band, we repeated the measurement at least 3 times, moving the camera vertically by approximately 1 cm each time. The resulting data set consists of several images of the top and bottom edges of each band, each image taken from a different height above the band. Acquiring multiple images ensured that we could interpolate the measurement to the same distance d relative to the band for each year. Although rearranging and integrating equation 2.1 shows that observed apparent radius varies with the inverse square of the distance d, over the short range of our survey the relationship is almost linear.

2.4.2 Data reduction

We first digitized the video images using a commercially available video frame grabber. We then found the radius of the band edge on each video image. Since the band was markedly darker than the surrounding firn, we used an edge detection process to enhance the edge of the band. After extraneous edges were removed, the apparent radius of the band was determined by fitting a circle to the bright pixels of the band edge, using a least-squares

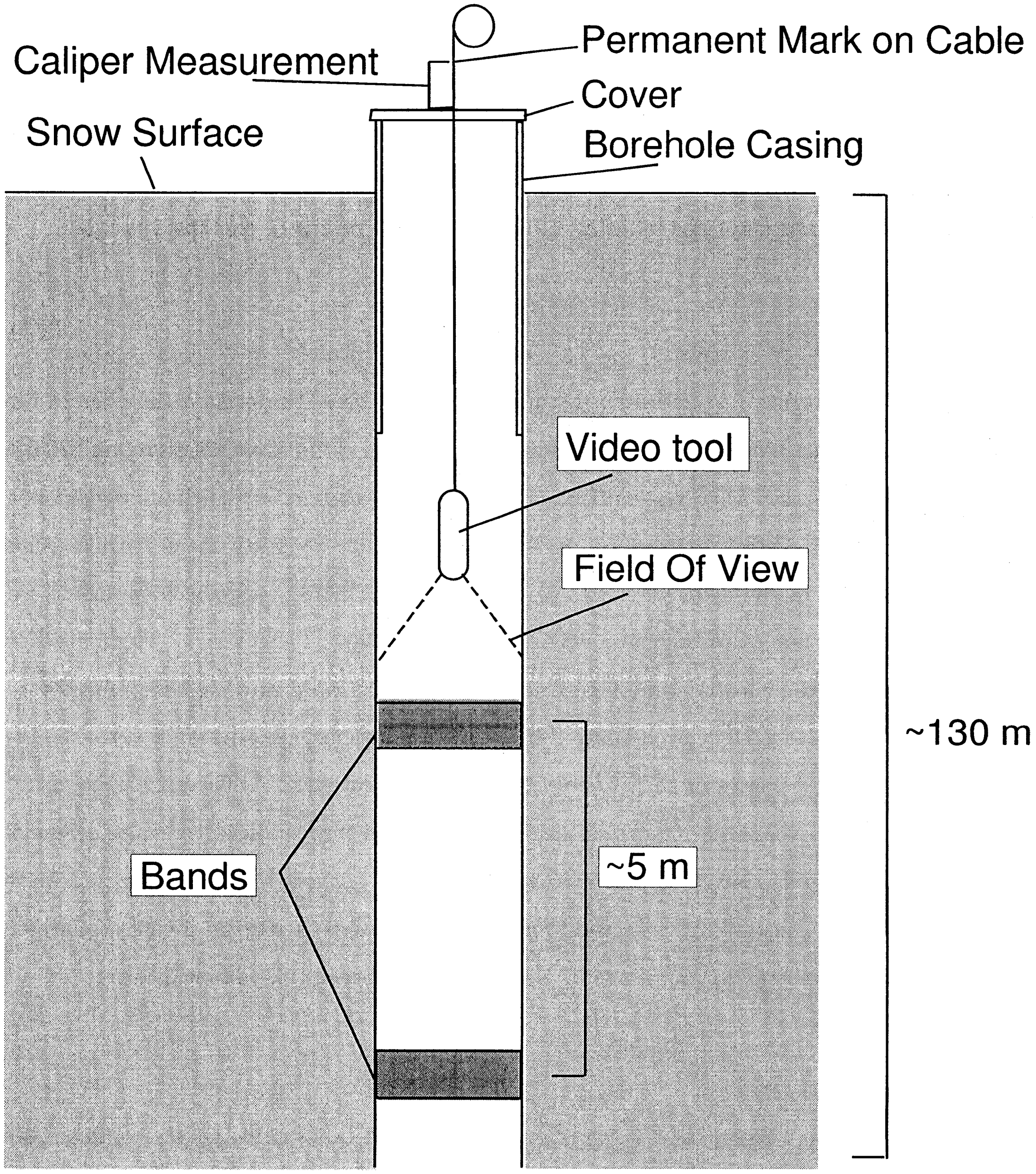

Figure 2.1: Schematic of the video tool in the borehole.

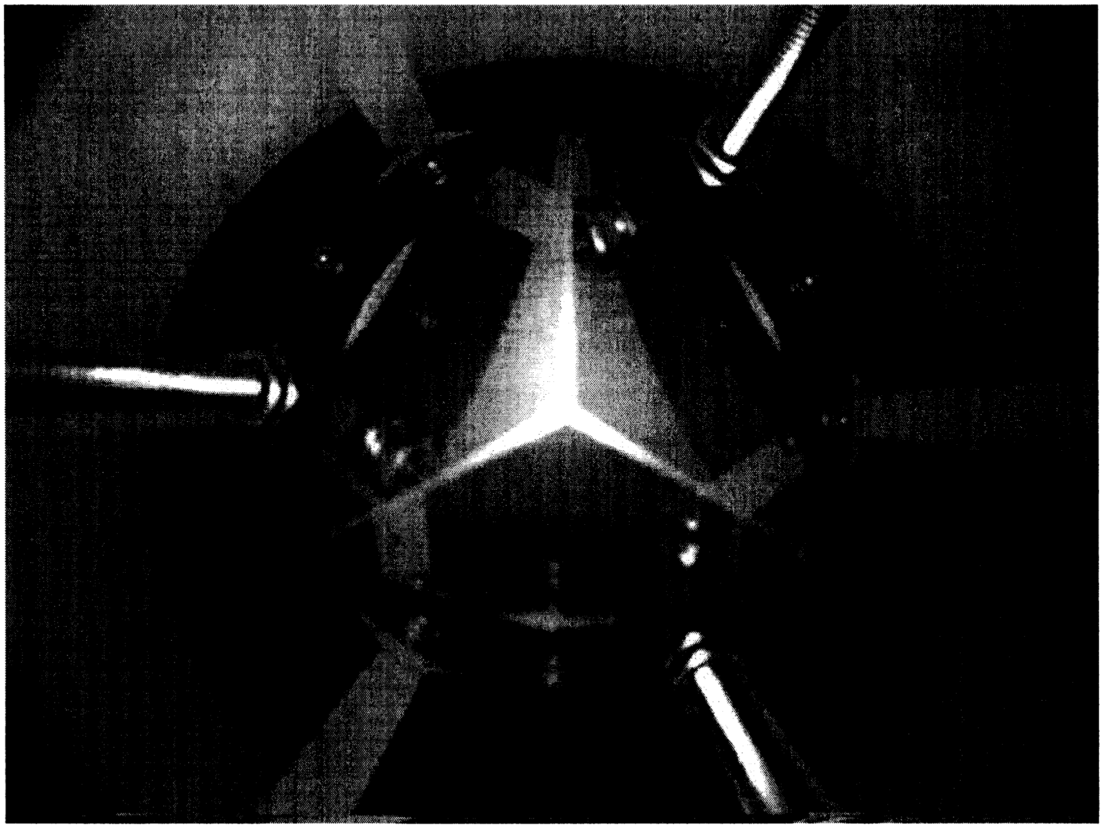

Figure 2.2: Downward-looking image of a band at ≈ 50 meters. In the center of the field of view is a corner reflector for looking directly out to the sides which was not used in this analysis. Only the direct image of the band (dark circle) was used.

process. For each band, we plotted the apparent radius of the band against the height of the permanent mark on the cable above the top of the borehole casing. The result (Figure 2.3) was an almost linear relationship. Repeating the process the following year gave a similar line at a different height. The offset between the 2 lines gives the displacement of the band relative to our reference mark (i.e. the top of the casing). This displacement divided by the elapsed time between measurements (approximately 1 year) gives relative velocity $w_r(z)$ between the borehole casing and the band at depth z.

2.4.3 Sources of error

Noise appears to grow sharply at depths greater than 85 meters. At these depths the decreasing contrast between the ice and band makes the band edge more difficult to distinguish in the video image. This source of error is addressed in the next section. Modifying the markers to have an easily visible edge would help to overcome this. In addition, since the expected signal for vertical strain becomes very small at these depths, the signal-to-noise ratio declines with depth. Bands such as the ones we used have slipped in past experiments (Raymond and others, 1994). Although we have no reason to conclude that bands were displaced in our experiment, it is impossible to exclude displacements smaller than ±2mm. A further uncertainty in this system is introduced by the cable. The plastic-sheathed video cable was not designed or tested for consistent elastic or thermal response, and the effects of aging are unknown. If the cable stretches by a certain amount one year and a different amount in a subsequent year, error is introduced. Since the stretch would be affected by the temperature profile along the cable, laboratory tests on the cable are impractical. Using an accurately calibrated logging cable that could carry a video signal would minimize this source of error.

2.5 Vertical Velocity

To obtain a vertical velocity profile for use in calculating a depth-age scale, we must address two issues: accounting for the uncertainty in our measurements, and converting our measured velocities relative to the top of the hole into absolute velocities.

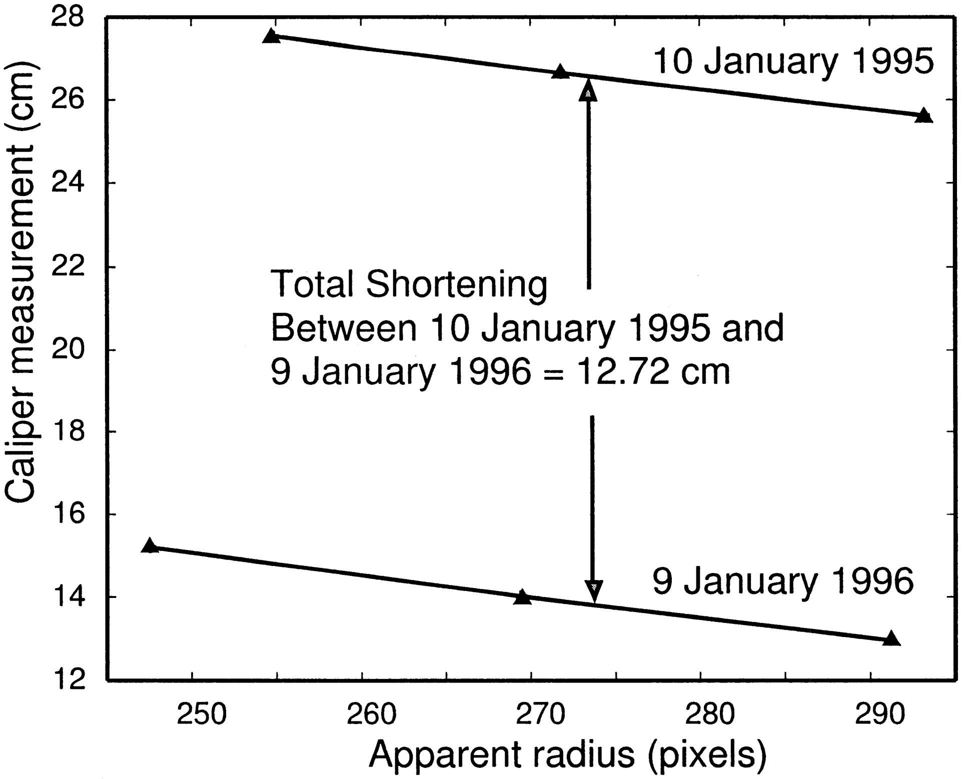

Figure 2.3: The observed apparent band edge radius in an image as a function of position of the logging tool. The caliper measures the distance from a mark on the cable to the top of the borehole casing. Separation between the two lines measures the total shortening of the firn column between 44.58 meters and the borehole casing.

For these calculations, we introduce three assumptions that we will also use in calculating density: 1) the density profile in the hole is in steady state (Sorge's law, Paterson, 1994, p. 14), such that

$$\nabla \cdot (\rho \vec{v}) = 0, \tag{2.2}$$

2) $\rho(z)$ is independent of x and y, and 3) The horizontal components of $\vec{v}(x, y, z)$ and therefore the horizontal strain rates are independent of depth z over the depth range of the survey. This last assumption is valid for the shallow depths we are concerned with here, where the largest motions are associated with firn densification. The combined divergence-driven horizontal strain, 1.3×10^{-4}, is an order of magnitude smaller than the vertical strain (1.3×10^{-3} at 25 meters).

2.5.1 Measurement uncertainty

To address the uncertainty in our measurement of $w_r(z)$ at depth, we define a new parameter γ. We expect a smoothly varying vertical velocity pattern. Below 85 meters, our velocity data have a much larger spatial variability than we would expect firn or ice to exhibit. As indicated above, this is likely due to difficulty in distinguishing band edges. A "least squares" smooth curve through the points might not reflect the true profile. Therefore we use physical constraints to extend our relative velocity curve below the last reliable points. Measured values of horizontal strain at the surface combined with conservation of mass provide a lower limit on the vertical strain rate below 80 meters. The magnitude of the vertical strain rate ($| \partial w/\partial z |$, the slope of the velocity curve) cannot be smaller than the total horizontal strain rate ($| \partial u/\partial x + \partial v/\partial y |$): unless the firn is dilating, material flowing out in the horizontal direction must be replaced by material from above. The upper limit is taken as a curve drawn through our highest relative velocity measurements. The true vertical velocity profile is then somewhere between the two extremes. We define the partitioning coefficient $\gamma, 0 \leq \gamma \leq 1$ as a measure of the position of the actual velocity profile $w_r(z)$ relative to the two extremes. Once a value of γ is chosen,

$$w_r(z) = \gamma w_r^l(z) + (1-\gamma)w_r^u(z), \tag{2.3}$$

where $w_r^l(z)$ and $w_r^u(z)$ are the lower and upper limits, respectively. The measured $w_r(z)$ data points, and the range of $w_r(z)$ profiles allowed by (2.3) are shown in Figure 2.4(a). A sampling of the measured w_r values are listed in table 2.1, along with measured densities.

2.5.2 Absolute velocity

Our goal is to arrive at a true vertical velocity for each surveyed point in the borehole, to be used in calculating a depth-age scale. For any given marker, the true vertical velocity is found by adding the measured velocity $w_r(z)$ relative to the surface marker to the absolute downward velocity w_o of the surface marker. For a steady surface, ideally we could measure w_o using survey-quality repeat GPS measurements such as those made by Hamilton and Whillans (1996). Since we do not have such data, we infer w_o using measured density profiles from the main core site 50 meters away.

Conservation of mass in a vertical column of ice from the surface to the depth z_{bot} of the borehole (here 130 meters) gives

$$w_o\rho_o - w(z_{bot})\rho(z_{bot}) = \left(\frac{\partial u}{\partial x} + \frac{\partial v}{\partial y}\right)\int_0^{z_{bot}} \rho(z)dz, \tag{2.4}$$

where ρ_o is the density of snow at the top of the hole. Fitzpatrick (1994) and Grootes and others (1994) measured density ρ as a function of depth z, and Morse (1997) measured the horizontal strain rate $(\partial u/\partial x + \partial v/\partial y)$ at the surface using a network of poles. Equation (2.4) says that in steady state, any mass that comes in the top of the box, and does not go out the sides, must come out the bottom.

Now, to express w_o entirely in terms of readily measurable quantities, we first recognize that $w_o = w(z_{bot}) - w_r(z_{bot})$, where we have already measured the relative velocity $w_r(z_{bot})$ of the bottom of the hole. Second, we note that the mass flux $w_o\rho_o$ through the upper surface of the ice sheet can also be written as $\dot{b}\rho_{ice}$, where $\dot{b}$ is ice-equivalent accumulation rate, and ρ_{ice} is the density of ice. Third, we note that the density $\rho(z_{bot})$ at the bottom of the hole has reached the ice density ρ_{ice}. Incorporating this information into (2.4) leads to

Table 2.1: Values of relative velocity w_r and density measurements ρ_1 from Fitzpatrick (1994) and ρ_2 from Grootes and others (1994). Final accepted $w(z)$ and expected w_ρ predicted by steady state and Sorges law are also shown.

$Depth(m)$	$w_r(ma^{-1})$	$\rho_1(gcm^{-3})$	$\rho_2(gcm^{-3})$	$w(ma^{-1})$	$w_\rho(ma^{-1})$
3.87	.017	-	-	0.203	-
9.41	.073	0.529	0.485	0.165	0.166
19.43	.101	0.573	0.569	0.138	0.138
29.44	.114	0.665	0.618	0.124	0.124
39.52	.123	0.702	0.677	0.115	0.114
49.82	.131	0.713	0.727	0.107	0.104
59.84	.139	0.788	0.771	0.099	0.096
69.77	.148	0.807	0.811	0.092	0.090
79.94	.151	0.856	0.846	0.086	0.086
90.16	.155	0.870	0.877	0.083	0.083
100.21	.164	0.884	0.871	0.080	0.080
110.55	.168	-	-	0.078	-
120.51	.162	-	-	0.077	-

$$w_o = \dot{b} - \frac{1}{\rho(z_{bot})}\left(\frac{\partial u}{\partial x} + \frac{\partial v}{\partial y}\right)\int_0^{z_{bot}} \rho(z)dz - w_r(z_{bot}). \tag{2.5}$$

We then use $\dot{b}$ and γ as free parameters in the density model described below.

2.5.3 Density profile

Since the firn is compressible, vertical velocity is coupled to firn compaction. We find w_o by selecting the pair of parameters $[\dot{b}, \gamma]$ that, when combined with our measured dw/dz and used in the calculations below, simultaneously produces a pair of coupled solutions $w(z)$ and $\rho(z)$ such that $\rho(z)$ best matches measured densities. We then accept that corresponding velocity solution $w(z)$.

Expanding (2.2) with the assumptions above, and then solving for $\partial\rho/\partial z$ in yields

$$\frac{\partial \rho}{\partial z} = -\left(\frac{\partial u}{\partial x} + \frac{\partial v}{\partial y} + \frac{\partial w}{\partial z}\right)\frac{\rho(z)}{w(z)} \tag{2.6}$$

which can be integrated numerically to obtain a density profile, using measured values of $\partial u/\partial x$, $\partial v/\partial y$, and $\partial w/\partial z$. We computed density distributions using a range of possible values for both $\dot{b}$ and γ. For each $[\dot{b}, \gamma]$ pair, we compared the modeled density profile to measured density data from the main borehole 50 meters away (Grootes and others, 1994; Fitzpatrick, 1994). Our preferred profile is the one that matches the measurements most closely in a least-squares sense. Equation 2.6 can also be solved to predict a $w(z)$ profile, based on a measured $\rho(z)$ profile and a surface velocity. Using a value for the surface velocity from our final accepted velocity profile (derived in this section), the resulting velocity profile w_ρ agrees well with our accepted final $w(z)$ profile; both can be seen in table 2.1. To quantify our confidence in our preferred profile, we use the "bootstrap" method (Press and others, 1992, p. 691).

2.5.4 Bootstrapping confidence levels

The goal of bootstrapping is to place confidence bounds on a measurement or on a calculated result, where the underlying sampled population cannot provide traditional statistical information. In the current situation, we look for confidence bounds on our calculated $w(z)$

and $\rho(z)$, yet we have only one density sample from any given depth and therefore cannot calculate a standard deviation for these underlying data. In the bootstrap method, the lack of repeated measurements is compensated for by using the actual data set D_0 to create a number of synthetic data sets $D_1, D_2, ...$, each with the same number of points as the original set. Each synthetic data set is populated by drawing samples at random from the measured data set *with replacement.* Replacement ensures that in the synthetic data sets, some measurements will be repeated (and thus be more highly weighted) and some will be omitted. For each of these synthetic data sets we find a "best fit" calculated density profile. The resulting set of "best fit" values of $\dot{b}$ and γ serve as a population from which we can calculate meaningful statistics. One such population of 224 sets of fitted parameters is shown in Figure 2.5, along with our resulting preferred value for $\dot{b}$ and its 95% confidence interval. This confidence interval is used to estimate the error range on the velocity profile and the associated depth-age scale discussed below.

The preferred velocity profile, shown by the bold curve in Figure 2.6, uses $\dot{b} = 0.0865$ m a^{-1} and $\gamma = 0.35$. The shaded region contains all profiles with $\dot{b}$ inside the 95% confidence interval in Figure 2.5.

Surface density measurements provide further support of our optimization. All model runs within our 95% confidence interval produced surface densities in the range 0.32 g $\text{cm}^{-3} \leq \rho \leq 0.35$ g cm^{-3}; these values fall within the range of measured surface densities at Taylor Dome (M. Duvall, unpublished field report, 1994).

2.6 Dating the core

We use the vertical velocity profile in Figure 2.6 to calculate a depth-age scale for the upper 130 meters, following the procedure used by Paterson and others (1977) for the Devon Island Ice Cap. We still assume that the vertical velocity profile is in steady state in a reference frame fixed to the surface, which could be moving up or down. Although the particle paths do not follow straight down the borehole, the horizontal components of $\vec{v}(x, y, z)$ are small enough that the vertical component is unlikely to vary with x or y and the one-dimensional approximation is valid.

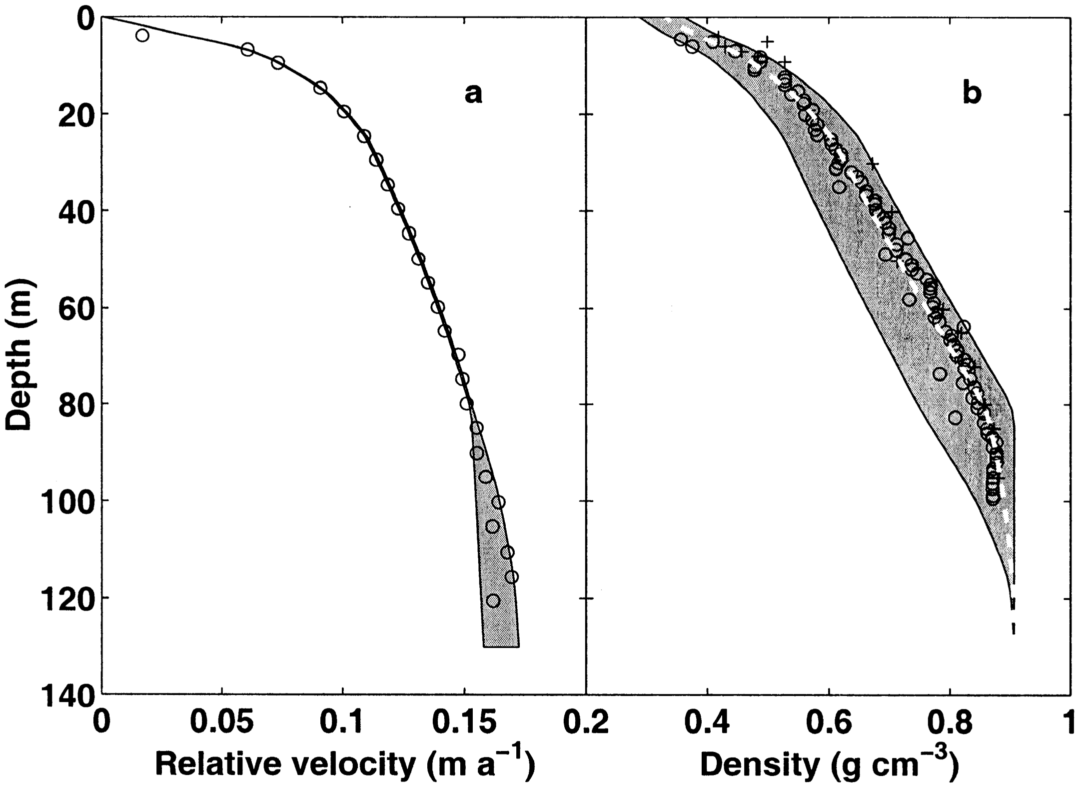

Figure 2.4: (a): The measured vertical motion of markers relative to the surface. The shaded grey area indicates the region encompassed by $0 \leq \gamma \leq 1$. (b): A modeled density profile (dashed line) compared to two measured density data sets from a hole 50 meters away. The modeled density is constrained to converge on that of pure ice (0.917 $g\ cm^{-3}$). The shaded grey area indicates the range of possible density depth profiles for $0 \leq \gamma \leq 1$.

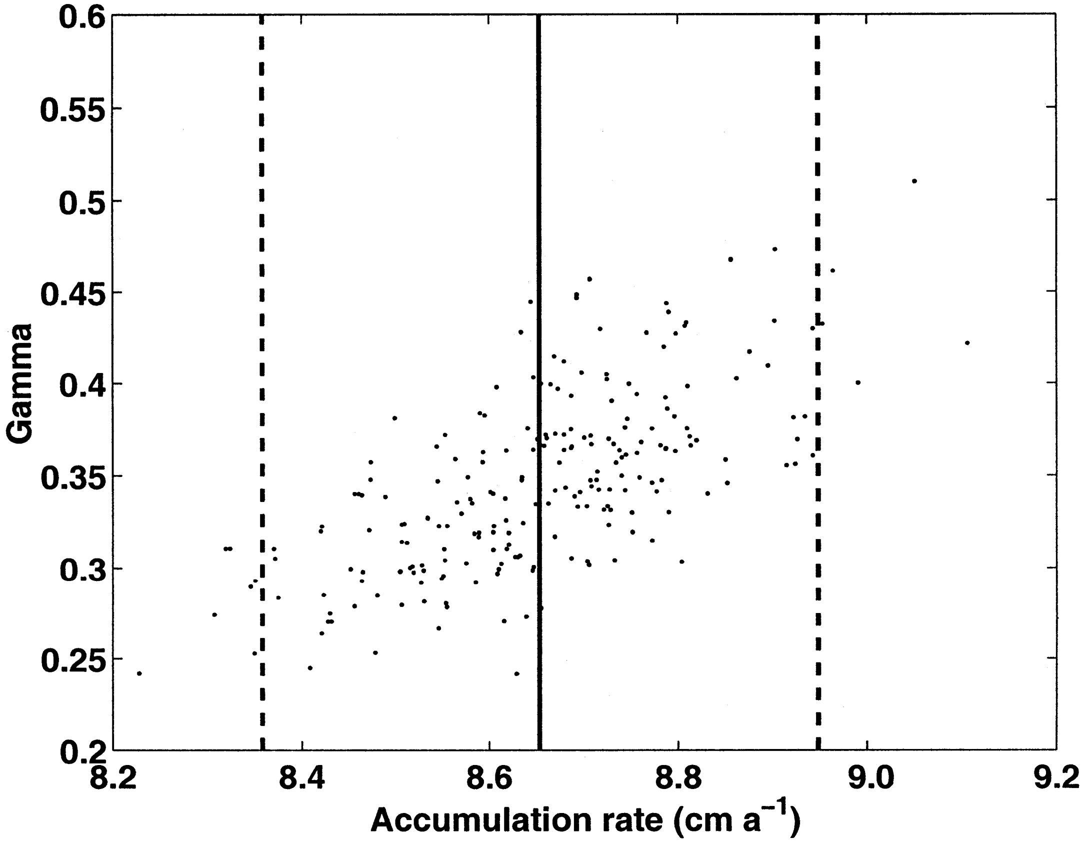

Figure 2.5: The population of 224 "bootstrapped" $\dot{b}$ and γ, the best fit $\dot{b}$ (solid vertical line) and 95% confidence interval on $\dot{b}$ (dashed vertical lines). $\dot{b}$ is indicated in ice equivalent units.

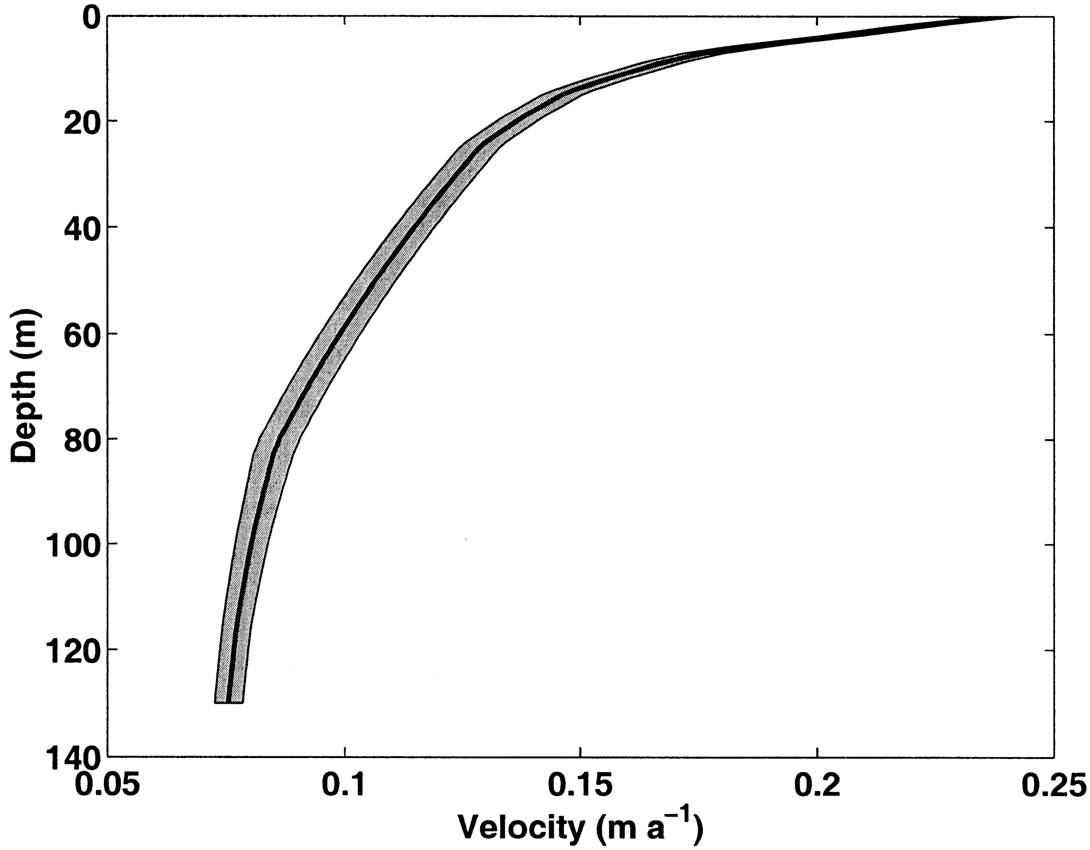

Figure 2.6: The vertical velocity profile. The bold line shows the best fit. The shaded region contains all profiles with $\dot{b}$ inside the 95% confidence interval in Figure 2.5.

We numerically integrate the inverse of the vertical velocity from the surface to depth z to find the age today of ice at depth z,

$$age = \int_0^z \frac{1}{w(\xi)} d\xi. \tag{2.7}$$

Using our preferred $w(z)$ profile, the resulting depth-age profile is shown by the bold curve in Figure 2.7. The shaded region on either side of the bold curve represents age profiles produced with the highest and lowest w_o values allowed by our 95% confidence interval in Figure 2.5.

2.7 Discussion

2.7.1 Accumulation rates

The range of accumulation rates within the 95% confidence interval in Figure 2.5 is compatible with local accumulation rates measured by a variety of methods (Morse and others, 1999). Our measurement provides a physical constraint on the average accumulation rate over the last 1300 years, in much the same way as gross-β measurements of nuclear bomb fallout products (see Picciotto and Wilgain (1963) for a description of the method) provide a constraint on average accumulation over the last ≈ 45 years.

Our 1300-year average value for $\dot{b}$ is greater than the 45-year average of $\dot{b} = 7.6$ cm a^{-1} from gross-β, and greater than the average of $\approx 6 - 7$ cm a^{-1} over the Holocene (Steig and others, 2000; Morse and others, 1998). Conservation of mass implies that a steady state ice dome with $\dot{b}$ throughout the Holocene equal to our value of 8.65 cm a^{-1} would require a larger horizontal flux divergence, either by being considerably thicker than Taylor Dome, or having greater horizontal strain rates than those measured by Morse (1997).

This illustrates the temporal variability of the accumulation rate pattern at Taylor Dome. Our analysis derives an average value of $\dot{b}$, whereas the true accumulation rate probably varied over time. Since the accumulation rate affects the slope of the depth-age curve, a calculation that allowed for a time-dependent accumulation rate would produce a depth-age profile which might show slope deviations of up to 10-20% from our preferred curve in Figure 2.7, but would on average produce similar ages at similar depths.

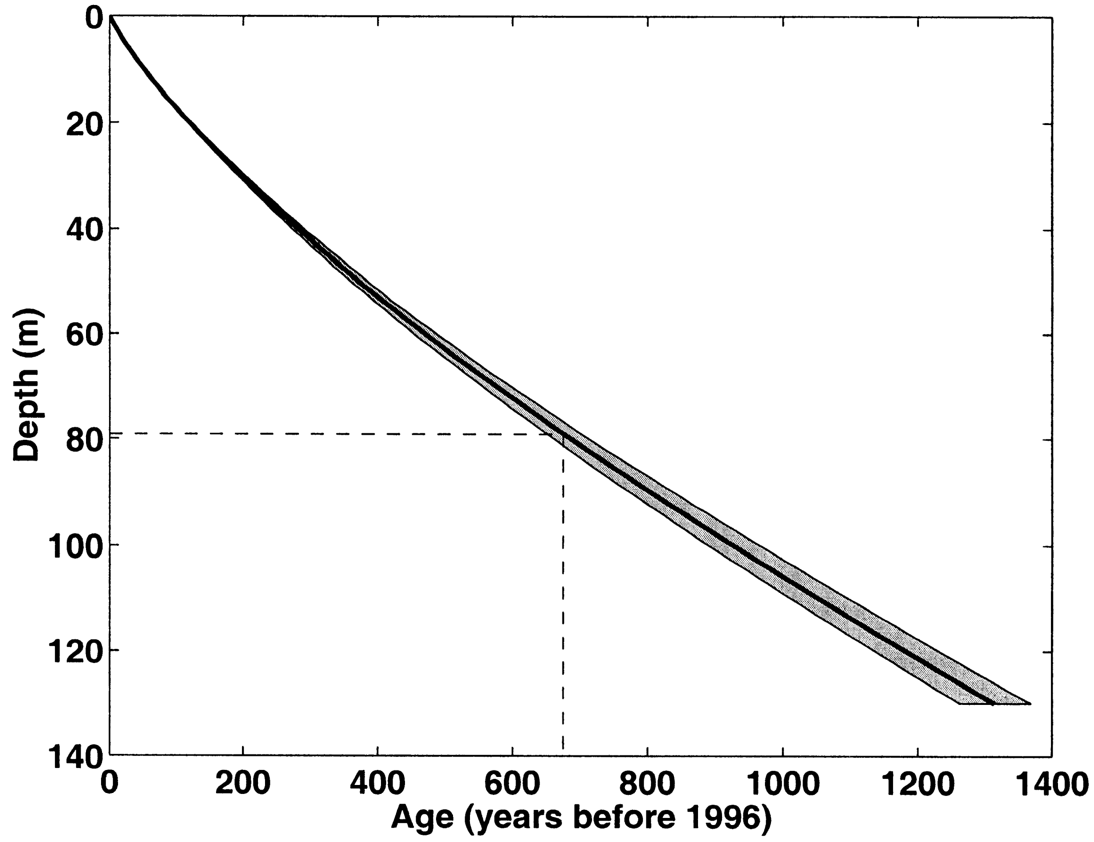

Figure 2.7: Depth-age scale for the firn at Taylor Dome C hole. The bold curve was made using the preferred accumulation of 8.65 cm a^{-1} and γ of 0.35. The shaded region represents the range of possible depth-age scales with $\dot{b}$ inside the 95% confidence interval in figure 2.5. The depth and age of a volcanic ash layer from a depth of 79.1 meters (675 ± 25years) are indicated by the dashed lines.

2.7.2 Ash layer

A number of primary volcanic ash, or tephra layers, are found in the ice cores from Taylor Dome and from Siple Dome, West Antarctica. Tephra layers, when found in sedimentary sequences such as ice, provide time-stratigraphic markers because volcanic eruptions, ash transport, and deposition occur in geologically-short time intervals. A well-defined and chemically distinctive tephra layer is found at a depth of 79.2 meters in the Taylor Dome ice core. Although this layer is interpreted to be from a local source volcano and cannot be directly dated, it is chemically indistinguishable from a layer found at a depth of between 97.2 and 97.7 meters in the Siple Dome B core. Based on the geochemical correlation, as well as the similarity of shard morphology, these layers are interpreted to be the result of the same volcanic eruption, and therefore to represent the same time interval in the two cores.

The age of the lowest horizon where the ash was found, 97.7 meters depth, in the Siple Dome A ice core has been estimated to be 709 years before 1995 with an error of 10% (K. Taylor, pers. comm., 2001), and we would infer that the 79.2 meter depth in the Taylor Dome core is the same age. This age is very close to the age determined by vertical strain measurements presented in this paper (675 ± 25 years before 1996, Fig. 2.7). The slight discrepancy between the ages may be in part due small errors in the age-depth estimates for the Siple Dome ice core.

2.8 Conclusions

Measurement of vertical velocity in an ice sheet borehole is possible with readily available hardware and software that can be used with few modifications. This is a useful measurement because it can provide a physically-based depth-age scale where the geochemical annual layer record is disturbed or unresolvable. Our calculated depth-age scale is likely the most accurate depth-age scale for the Taylor Dome firn thus far, and can also help constrain dating of the Siple Dome core.

Chapter 3

VERTICAL STRAIN MEASUREMENTS IN FIRN AT SIPLE DOME, ANTARCTICA

This chapter is in press under the same title in *Journal of Glaciology* with co-authors Edwin D. Waddington, Gregg W. Lamorey, and Kendrick C. Taylor. Kurt Cuffey, Gordon Hamilton, and Richard Alley provided helpful review comments. The specific contributions of my co-authors were as follows: Ed Waddington initiated the Siple Dome ice-dynamics project, helped guide my research, and edited the manuscript. Gregg Lamorey and Ken Taylor provided supporting data (a density profile and a depth-age profile, respectively) that I used in validating my results.

3.1 Summary

We measured vertical strain in the firn at Siple Dome, Antarctica, using two systems, both of which measure relative displacements over time of metal markers placed in an air-filled borehole. One system uses a metal-detecting tuned coil, and the other system uses a video camera to locate the markers. We compare the relative merits of the two systems. We combine steady-state calculations and a measured density profile to estimate the true vertical-velocity profile. This allows us to calculate a depth-age scale for the firn at Siple Dome. Our steady-state depth-age scale has ages ≈ 10-15% younger at any given depth when compared to depth-age scales derived by layer counting in a core 40 meters away. The age of a visible ash layer at 97 meters in the core is 665 ± 30 years, in agreement with a similar analysis conducted at Taylor Dome, Antarctica, where the same ash is also seen, providing an additional dated tie-point between the 2 cores.

3.2 Introduction

Measurements of vertical strain can add valuable information to a glaciological field program. Several methods of measuring vertical strain in firn and ice have been described

(Hamilton and others, 1998; Zumberge and others, 2002; Elsberg and others, 2004, in review). However, most are primarily point-measurements- detailed measurements of vertical strain in the firn are rarely made. Such measurements can provide insight into the mechanics of firn compaction by constraining the actual rates of compaction, and they can be used to assign a depth-age relationship to the shallow sections of an ice core. This depth-age relationship, when combined with independent depth-age scales from other methods, can shed light on the possibility of transient variations in accumulation and surface density.

Siple Dome is an ice dome on the Siple Coast of West Antarctica, latitude 81.65° South and longitude 148.81° West. It is an "inter-ice-stream ridge"; the dome is a flow divide situated in slow-moving ice between the Kamb and Bindschadler ice streams. In the austral summers of 1997-1999, an ice core was drilled 1004 meters to bedrock. In addition to the main core, several smaller shallow cores were drilled. We made our vertical strain measurements in an auxiliary borehole, which was 105 m deep and located 40 meters from the main core site.

3.3 Measurements

We made vertical-strain measurements using 2 different methods. We placed metal bands in the borehole at roughly 5-meter intervals, and surveyed the locations of the bands over the course of three annual field seasons. We determined the location of a band both with a "metal detector" tuned resonating inductive coil, and with a downward-looking borehole video camera. The tuned coil and the video camera provide different means of measuring the relative displacement of a band.

3.3.1 Marking bands

Each metal marking band is a strip of bronze spring stock, 10 cm wide and 1 m long (c.f. Rogers and LaChapelle, 1974; Raymond and others, 1994; Hawley and others, 2002). The strip is coiled on a custom injector tool and lowered into the borehole. When the band is released, it expands to press against the sides of the borehole. The logging tools can then pass through the coiled band to observe other bands at greater depths. In practice, the injection of the bands is time consuming and difficult. At Siple Dome, the band at 84 meters was snagged during the first logging run. Although we were able to free our logging tool, we did not attempt to re-log this band or the others below it until the final season of the project.

3.3.2 Tuned Coil

The tuned-coil detector was built to a modification of the design presented in Rogers and LaChapelle (1974), based on the suggestions of Raymond and others (1994). It is essentially a metal detector, in which a circuit drives a signal through a coil, which is designed to produce resonance in the absence of nearby conductors. As the coil is brought close to a conductive object (in our case a metal band), current is induced in that object, and the resulting mutual inductance "detunes" the detector. This results in reduced resonance. The theory of the instrument is documented by Rogers and LaChapelle (1974) and Raymond and others (1994). In practice, our tool is slightly "detuned", so that resonance first increases when approaching a marker, and then decreases as the tool enters the band. This provides more structure in the record for correlation. We suspended the instrument on a commercially-available steel measuring tape with 2 conductors embedded in its edges to carry the signal. The voltage signal from the tool was recorded with a data logger. Upon reaching a band, we clamped a linear displacement transducer to the tape. The transducer allows very fine-scale measurement of depth over the short range spanning a marking band. In combination with the readings from the tape where the transducer was clamped, the result is a very accurate depth measurement. The transducer output was also recorded by the data logger. On the resulting voltage vs. depth record (Figure 3.1), the signal from the band is very distinct.

3.3.3 Video

We also located the bands with a downward-looking borehole video camera, using the technique described by Hawley and others (2002). For the first log, we made a permanent mark on the cable when we could image each band. We measured the distance between this mark

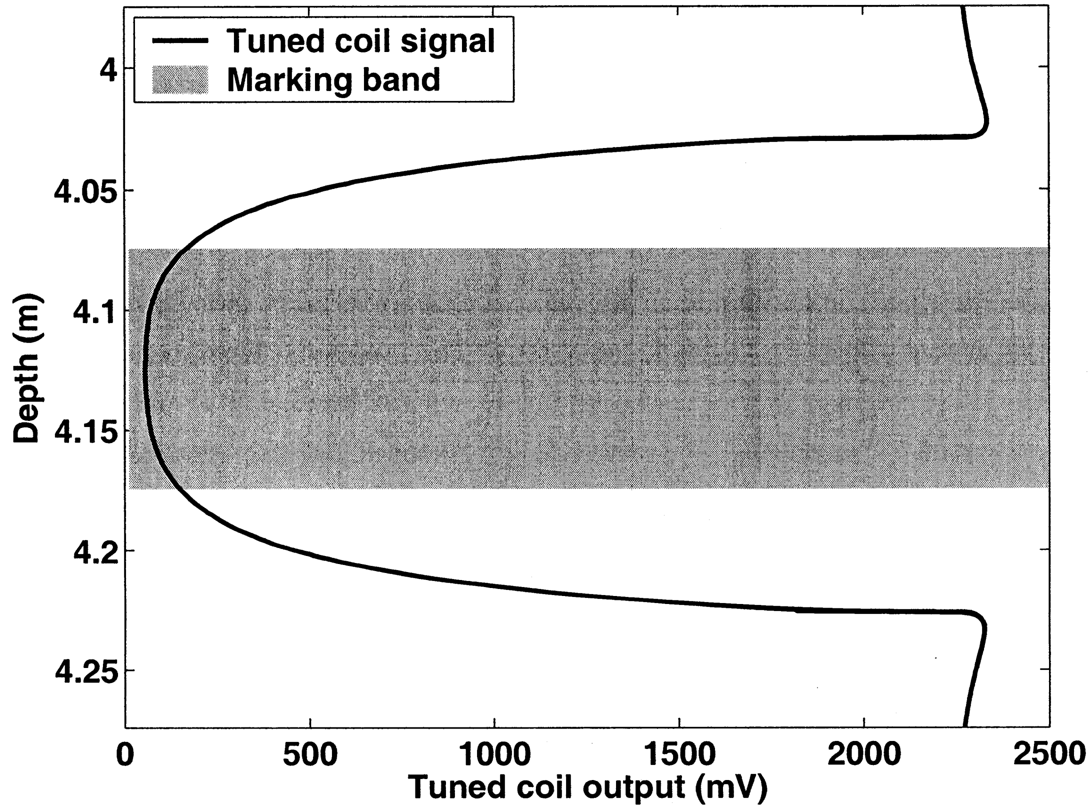

Figure 3.1: Voltage output from the tuned-coil detector as it is lowered through a typical metal marking band (marked by the shaded area). Because the coil is not optimally tuned in free space, the resonance first increases when approaching the band, then decreases to a minimum when the tool is centered inside the band.

and the top of the borehole casing with a vernier caliper for this and all subsequent images of this particular band edge.

The image of a band in the hole shows the edge of the band as a circle. We determine the location of the camera relative to the band by measuring the observed apparent radius of the band at a given camera position. The distance d between the camera lens and the edge of the band can be expressed in terms of the focal length f of the lens, the actual radius of the band r_a,and the observed radius of the band r_o:

$$d = \frac{f r_a}{r_o}. \tag{3.1}$$

Ideally we would select an optimum distance from each band to position the camera for caliper measurements, calculate the desired apparent radius r_d for that distance, and make the caliper measurement when the camera is positioned so that $r_o = r_d$. Since we did not have fine adjustment ability to position our tool, and had no accurate means of assessing the apparent radius in the field, we used the following "bracketing" approach to ensure we had positioned the camera in the same way from year to year.

For each band, we repeated the measurement at least 3 times, moving the camera vertically by approximately 1 cm each time. The resulting data set consists of several images of the top and bottom edges of each band, each image taken from a different height above the band. Acquiring multiple images ensured that we could interpolate the measurement to the same distance d relative to the band for each year. Although rearranging and integrating equation 3.1 shows that observed apparent radius varies with the inverse square of the distance d, over a short range of d ($\approx$3 cm in our case) the relationship is almost linear.

3.3.4 Density

Density measurements were made on the "SDM-B" core, taken 40 meters from the vertical-strain site. The density was determined by field measurements of the mass, length, and diameter of ice-core sections approximately one meter in length. Two length measurements were made to the nearest millimeter using a metal ruler, and then averaged. In the case of angled breaks between sections, a minimum and a maximum length were measured and then averaged. The diameter was measured to the nearest 0.1 mm using digital calipers at three locations along the core section and these were also averaged. The mass was measured to the nearest gram using a triple-beam balance.

3.4 Data reduction

3.4.1 Tuned coil

The output from the tuned coil is saved in the form of a depth-voltage series for each band. To locate the midpoint of each band, previous users of this method (Rogers and LaChapelle, 1974; Raymond and others, 1994) chose a point midway between 2 "threshold" points of equal voltage on the sharply rising or falling voltage curve. In our analysis, we use the entire record. To compare two records of a given band from different years, we first normalize each curve to eliminate any effect of different temperatures or battery voltage on the amplitude of the signal. Then we cross-correlate the two records. The offset producing the best cross-correlation is accepted as the relative displacement during the time interval between the records.

The band at 84 meters was dislodged so as to partially block the borehole in the first season before we used the tuned-coil tool. Because the tuned-coil tool is large, we were unable to make tuned-coil measurements below a depth of 79 meters.

3.4.2 Video

To find the radius of the band edge on each video image, we used an edge detection process to enhance the edge of the band. After extraneous edges were removed, the apparent radius of the band was determined by fitting a circle to the bright pixels of the band edge, using a least-squares process. For each band, we plotted the apparent radius of the band against the height of the permanent mark on the cable above the top of the borehole casing. The result was an almost linear relationship. Repeating the process the following year gave a similar line at a different height. The offset between the 2 lines gives the displacement of the band relative to our reference mark (i.e. the top of the casing).

We improved the band-edge detection algorithm; in the previous method we applied a numerical edge-detection filter and then manually removed extraneous edges in the image (such as parts of the camera that were in the field of view) before fitting a circle to the remaining bright pixels. The present method masks out the extraneous edges, and then fits a circle in several iterations, each time removing edge-detected pixels several standard deviations away from the best-fit circle. This removes reliance on the operator to find and remove all "noise" pixels. We believe that this improved the accuracy of the results at greater depths where reduced image contrast was previously a limitation.

3.4.3 Density

The largest source of uncertainty in the density measurements is missing pieces of unknown mass and volume due to breaks in the ice core. These sections of core were omitted from the density data set. Another source of uncertainty is the length measurement where there was an angled break between adjacent sections. The average density for these adjacent sections often provided a reasonable density value. However, if the average density of a core section containing an angled break produced a suspect value, it was omitted from the density dataset. Densities have been interpolated for the ice-core sections with omitted values. The standard deviation of the density measurements is estimated to be 0.005 gm cm^{-3}. Below 70 meters, the data show more noise; we expect this to be associated with missing pieces of core, resulting in low values.

3.5 Vertical velocity

Our data analysis produces depth profiles of relative velocity, and of density, shown in Figures 3.2 and 3.3. Because we did not have data from the tuned-coil detector below 75 meters, we use the video data for vertical velocity and depth-age scale analyses. We measured displacements, and hence velocity, relative to the borehole casing, which was attached to a plywood board at the surface and extended $\approx$1 m into the borehole. To convert to absolute velocity for use in calculating a depth-age scale, we follow the procedure of Hawley and others (2002). We start with our relative velocity, add an estimate of the true velocity of one point in the borehole, use conservation of mass to calculate a density profile with that velocity, and compare that to our measured density profile. We accept vertical velocity estimates that result in a close match between measured and modeled densities.

For our calculations, we introduce three assumptions: 1) The horizontal components $u(x)$ and $v(y)$ of the total velocity vector $\vec{V}(x, y, z)$, and therefore the horizontal strain rates, are independent of depth z over the depth range of the survey. 2) The density $\rho(z)$ at a given depth is independent of horizontal position x and y. 3) the density profile in the borehole is in steady state (Sorge's law, Paterson, 1994, p. 14), such that

$$\nabla \cdot (\rho \vec{V}) = 0. \tag{3.2}$$

The first assumption is valid for the shallow depths that we are concerned with here, where the largest motions are associated with firn densification. From horizontal strain measurements at the surface (Nereson, 1998) we know the total horizontal strain rate, which we indicate here as $\partial u/\partial x + \partial v/\partial y$.

For any given marker, the true vertical velocity is found by adding its measured velocity $w_{\mathrm{r}}(z)$ relative to the surface marker to the absolute downward velocity w_{o} of the surface marker.

Conservation of mass (Equation 3.2) in a vertical column of ice from the surface to a depth z' in the borehole (here 100 meters) gives

$$w_{\mathrm{o}}\rho_{\mathrm{o}} - w(z')\rho(z') = \left(\frac{\partial u}{\partial x} + \frac{\partial v}{\partial y}\right) \int_0^{z'} \rho(z) dz, \tag{3.3}$$

where ρ_{o} is the density of snow at the top of the borehole.

Now, to express w_{o} entirely in terms of readily measurable quantities, we first recognize that $w_{\mathrm{o}} = w(z') - w_{\mathrm{r}}(z')$, where we have already measured the relative velocity $w_{\mathrm{r}}(z')$ at the bottom of the borehole. Second, we note that the mass flux $w_{\mathrm{o}}\rho_{\mathrm{o}}$ through the upper surface of the ice sheet can also be written as $\dot{b}\rho_{ice}$, where $\dot{b}$ is ice-equivalent accumulation rate, and ρ_{ice} is the density of ice.

Third, we assume that the density $\rho(z')$ at the bottom of the borehole has reached the ice density ρ_{ice}. Incorporating this information into (3.3) leads to

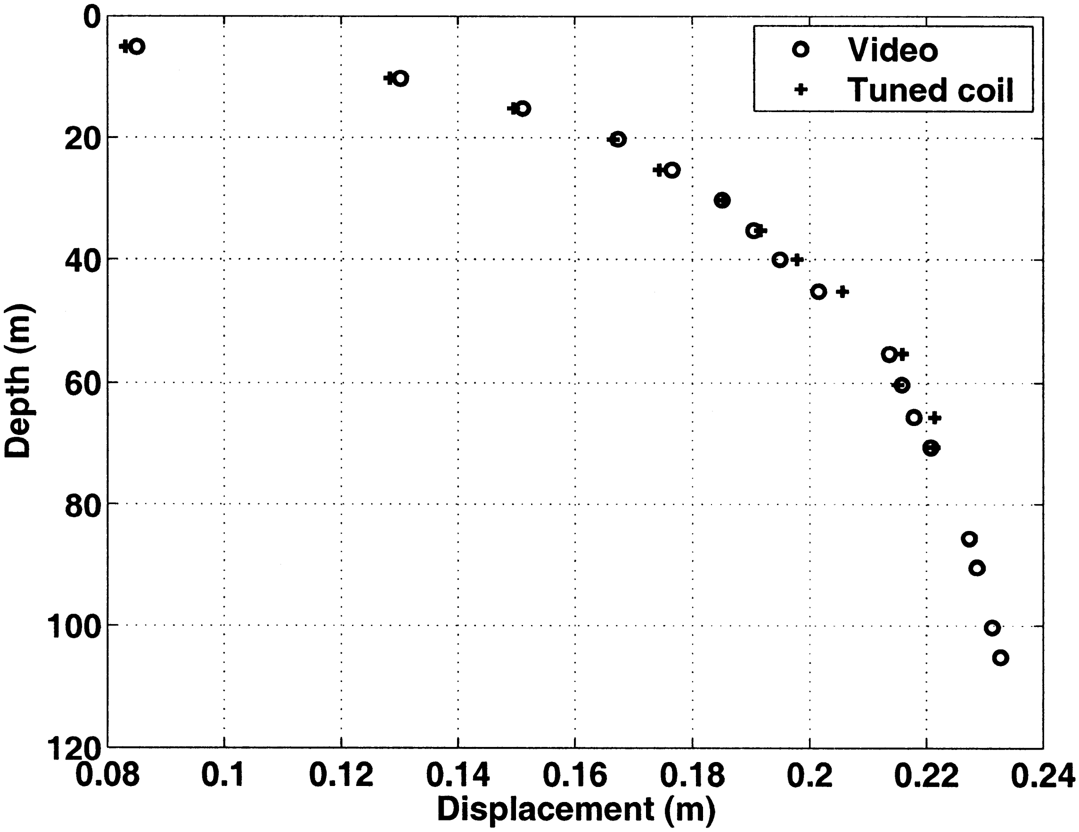

Figure 3.2: Annual vertical displacements averaged over two years measured with both the video and tuned-coil tools. All motion is referenced to zero at the top of the borehole casing. The noticeable break in slope around 60 m is due to the change in densification rate at that depth.

$$w_{\mathrm{o}} = \dot{b} - \frac{1}{\rho(z')}\left(\frac{\partial u}{\partial x} + \frac{\partial v}{\partial y}\right)\int_0^{z'} \rho(z)dz - w_{\mathrm{r}}(z'). \tag{3.4}$$

We then use $\dot{b}$ as the free parameter in the density model described below. In practice, the measured density at the bottom of our borehole did not reach the density of bubble-free ice, and so an additional factor of $\rho_{ice}/\rho(z')$ is included in the calculation of w_{o} to account for this.

Since the firn is compressible, vertical velocity is coupled to firn compaction. We find w_{o} by selecting the $\dot{b}$ that, when combined with our measurements and used in the calculations below, simultaneously produces a pair of coupled solutions $w(z)$ and $\rho(z)$ such that $\rho(z)$ best matches measured densities. We then accept that corresponding velocity solution $w(z)$.

Expanding (3.2) with the assumptions above, and then solving for $\partial\rho/\partial z$ yields

$$\frac{\partial \rho}{\partial z} = -\left(\frac{\partial u}{\partial x} + \frac{\partial v}{\partial y} + \frac{\partial w}{\partial z}\right)\frac{\rho(z)}{w(z)} \tag{3.5}$$

which can be integrated numerically to obtain a density profile, using measured values of $(\partial u/\partial x + \partial v/\partial y)$ and $\partial w/\partial z$. We computed density distributions using a range of possible values for $\dot{b}$ in equation (3.4) when computing $w(z)$. For each $\dot{b}$, we compared the modeled density profile to measured density data. Our preferred profile is the one that matches the measurements most closely in a least-squares sense. This preferred profile is shown along with the measured densities in figure 3.3. For each modeled density profile, we calculated a mismatch index

$$J = \sqrt{\frac{1}{N}\sum_{i=1}^{N}\left(\frac{(\rho_i^{\mathrm{d}} - \rho_i^{\mathrm{m}})}{2\sigma}\right)^2} \tag{3.6}$$

Where ρ_i^{d} and ρ_i^{m} are the density data and modeled density at the ith depth, respectively, N is the number of samples, and σ is the standard deviation of the measurements (estimated earlier as 0.005 gm cm^{-3}). J tells us how closely we match the density data with our model. $J = 1$ means that we have on average matched the data within 2 standard deviations. Figure 3.4 shows the relation between $\dot{b}$ and J. We accept models producing $J < 1$.

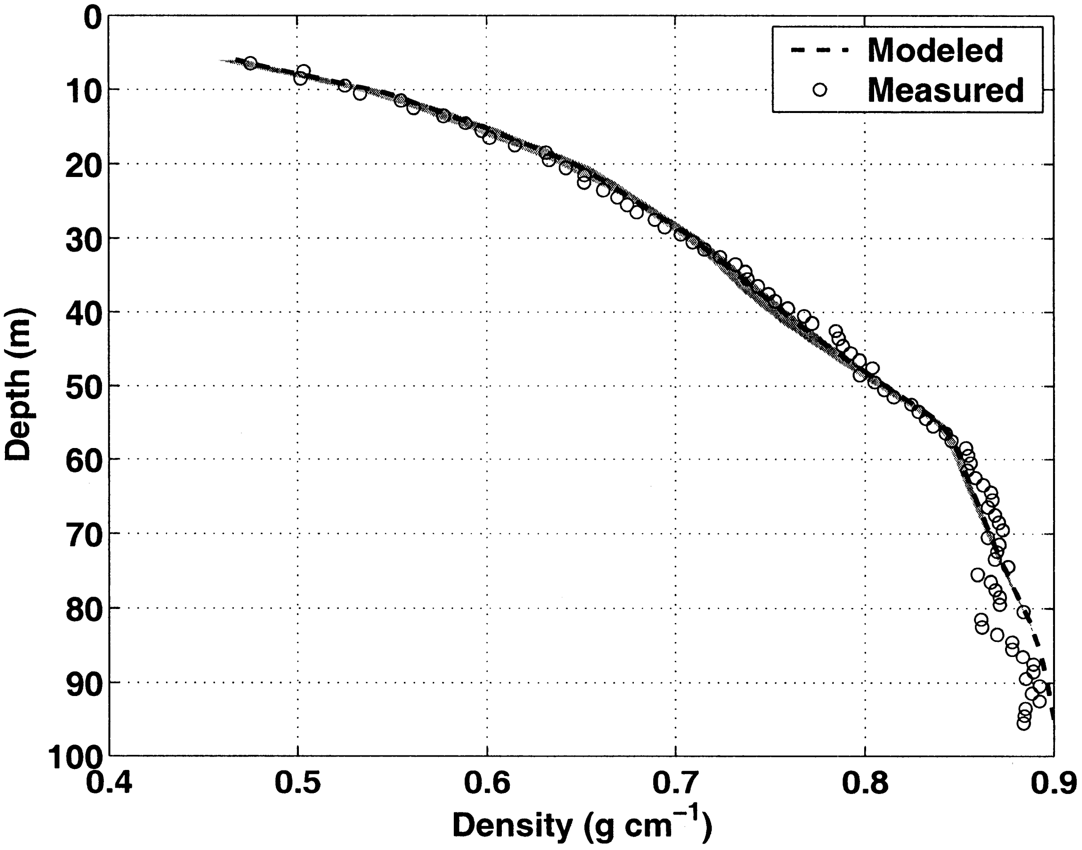

Figure 3.3: Density data (circles) from the Siple Dome "B" core and our preferred "best-fit" modeled density profile (solid curve) using $\dot{b} = 0.126$ m a^{-1}. The shaded region contains all modeled density profiles that match the data better than our mismatch threshold of J=1. These solutions correspond to a range of 0.12 - 0.133 m a^{-1} (ice equiv.) for $\dot{b}$. The narrowness of this region illustrates the relative insensitivity of our steady-state mass conservation model to differences of under 10 percent in accumulation rate.

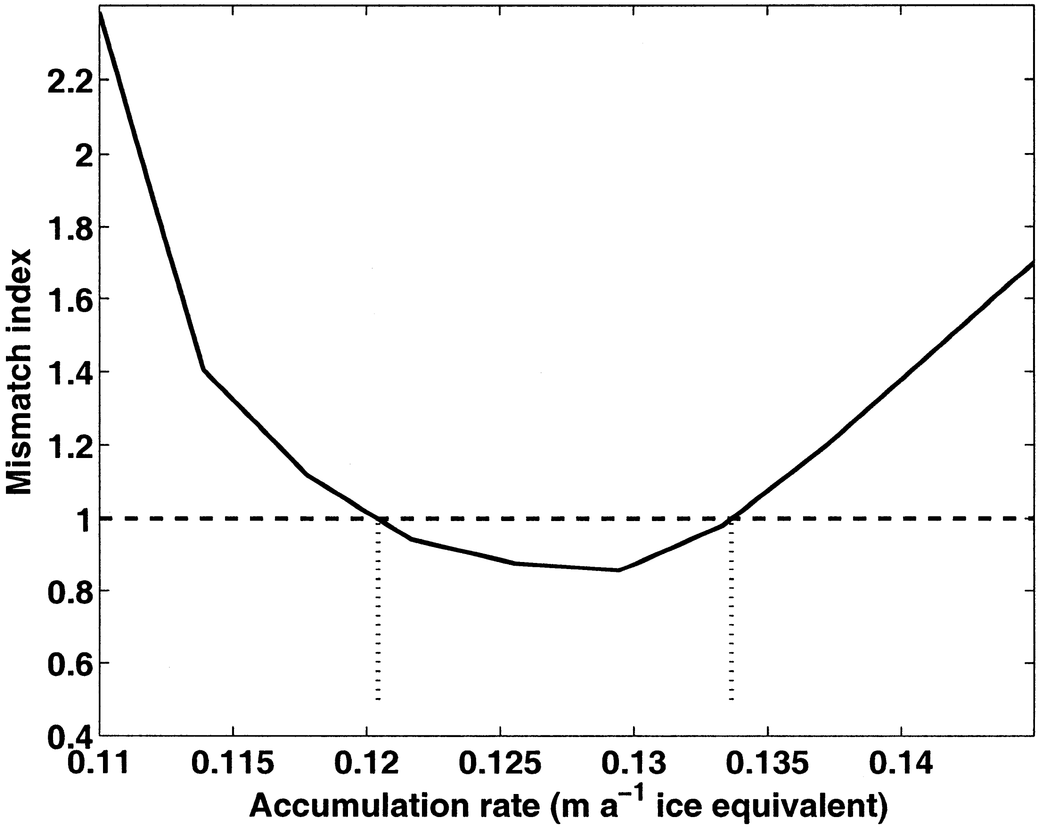

Figure 3.4: Mismatch index J (Equation 3.6) versus $\dot{b}$ for our density model. Our preferred "best fit" model uses $\dot{b}$ at the minimum J. We accept any result with a mismatch index $J < 1$.

3.6 *Depth-age scale*

We use the vertical-velocity profile to calculate a depth-age scale for the upper 100 meters, following the procedure used by Paterson and others (1977) for Devon Island Ice Cap, and by Hawley and others (2002) for Taylor Dome, Antarctica. We assume that the vertical velocity profile in the firn is in steady state in a reference frame fixed to the surface, which could be moving up or down due to changes in the thickness of the underlying ice. Although the particle paths are not precisely vertical, the horizontal components of $\vec{V}(x, y, z)$ are small enough that the vertical component is unlikely to vary significantly over the range of x or y spanned by the particle paths, so the one-dimensional approximation is valid.

We numerically integrate the inverse of the vertical velocity from the surface to depth z to find the age today of ice at depth z,

$$Age = \int_0^z \frac{1}{w(\xi)} d\xi. \tag{3.7}$$

Using our preferred $w(z)$ profile, the resulting depth-age profile is shown by the bold curve in Figure 3.5. The shaded region on either side of the bold curve represents age profiles produced with all w_o values allowed by accepting only density models giving $J < 1$ (as seen in Figure 3.4). Also shown for comparison are depth-age profiles determined using two layer-counting methods. In one method (PSU), annual horizons in a core from 40 m away were visually counted to determine age (R. B. Alley, Personal Communication, 2003). In the other method (Taylor and others, 2004, in review), a computer algorithm was used to interpret annual layers using electrical conductivity measurements made on the same core.

3.7 *Discussion*

3.7.1 Comparison of the two methods

The tuned-coil and video methods locate a marker in the borehole in different ways, and the opportunity to use the techniques side-by-side allows us to make comparisons. There are several benefits to using the tuned coil. The procedure for locating a band in any given record is straightforward and gives a robust indication of the location of the band. The tool,

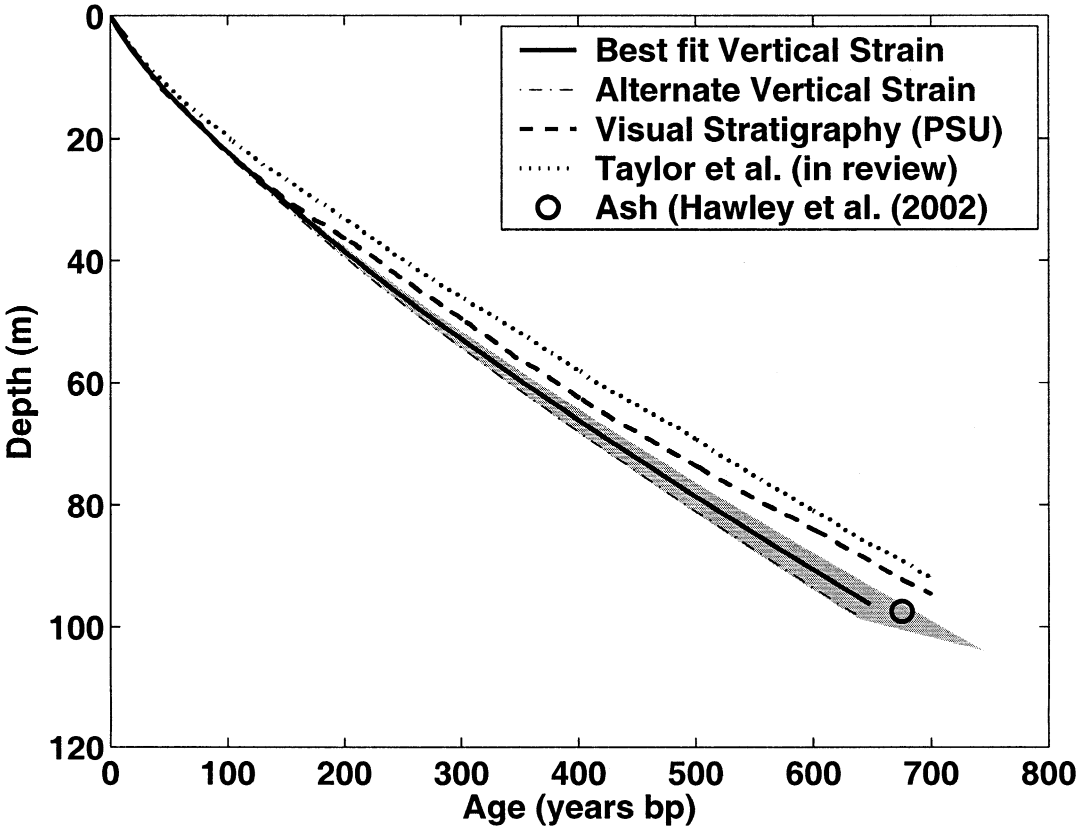

Figure 3.5: Depth-age scale for the firn at Siple Dome. The solid curve uses our preferred accumulation of 0.126 m a^{-1}. The shaded region represents the range of possible depth-age scales with $\dot{b}$ giving $J < 1$. The dash-dot curve uses accumulation of 0.132 m a^{-1} from Hamilton (2002). A volcanic ash layer at 97.5 meters was also seen at Taylor Dome, Antarctica (Dunbar and others, 2003). Its age of 675 years as dated at Taylor Dome by Hawley and others (2002) is indicated by the circle. Also shown are two independent depth-age scales for a nearby ice core, determined by counting visible annual layers (data from Pennsylvania State University, R. B. Alley, personal communication 2003), and by counting annual stratigraphy in electrical conductivity records (Taylor and others, 2004, in review). Our depth-age profile is younger on average, but within 10-15% of the others.

however, must be custom-built and cannot perform other functions. It is bulkier than the video tool, partly because the distance between the tool and the band on the borehole wall needs to be small. This distance requirement also means that different tools are needed for logging boreholes of different diameters.

With the video tool, we can inspect the condition of the borehole and the markers in real time. We use an unmodified commercial pipe-inspection camera, mounted on a simple frame. Data reduction with the video method is not straightforward, resulting in many steps between the raw video log and the vertical-strain result (Hawley and others, 2002).

The measured displacements from the two techniques agreed well, generally within a few millimeters. Both techniques require similar amounts of field time for a log. The limiting factor with both measurement types is probably the metal marker bands. They are difficult and time-consuming to place, and most importantly, they can be dislodged and block the borehole.

While our two methods span the firn at Siple Dome, there have been deeper vertical strain measurements made with optical fibers and wire strain meters. There is a small overlap between our shallow measurements and the deep measurements. Our shallow measurements agree closely with the deep measurements of both total vertical strain over the upper 80 meters (Zumberge and others, 2002), and strain at a depth of 80 meters on the $\approx$1 m scale of the wire strain meters (Elsberg and others, 2004, in review), improving confidence in both systems of measurement.

3.7.2 Steady-state assumption

Our estimated ages are consistently younger than those from annual layer counts in the nearby ice core. One reason may be that our calculation assumes steady-state accumulation, with a $\approx$ 700-year average of 0.126 m a^{-1}. In figure 3.5 we also show for comparison the depth-age profile generated using a $\dot{b}$ of 0.132 m a^{-1}, the 42-year average accumulation from Hamilton (2002). A profile generated using the minimum $\dot{b}$ suggested by the $1-\sigma$ uncertainty of 0.014 m a^{-1} quoted by Hamilton (2002) lies between our region of $J < 1$ and the PSU layer counted age, while a profile generated using the maximum $\dot{b}$ suggested by the uncertainty is substantially younger than our preferred profile. Solving equation (3.7) with a velocity profile generated using a $\dot{b}$ that is 10-15% lower than our preferred value brings the depth-age profile closely in-line with the layer-counted ages. However, when we use a 10-15% lower $\dot{b}$ in our density model, the modeled densities do not fit as well with the measured densities. This inconsistency may indicate that Siple Dome is in fact not in steady state, but rather has had some non-steady accumulation or surface density history which we cannot identify in this steady-state analysis. Furthermore, our approach in which we match the modern density profile may be insensitive to such transients. There are spatial gradients in accumulation at Siple Dome (Nereson, 1998; Hamilton, 2002), but they are small enough over a 40 m interval (≈0.2%, linearly interpolated) that spatial accumulation patterns cannot explain the discrepancy. Further study into detection of transients in accumulation or surface density using firn densification models (e.g. Spencer and others, 2001) could shed more light on the accumulation-rate and surface-density history of Siple Dome through the last millennium.

3.7.3 Ash Layer

An ash layer is visible in the Siple Dome core at ≈97.5 meters (Dunbar and others, 2003). This ash has been geochemically correlated with an ash layer at Taylor Dome, Antarctica (Hawley and others, 2002; Dunbar and others, 2003). At Taylor Dome, Hawley and others (2002) dated the ash layer at 675 ± 25 years using vertical-strain measurements and analysis similar to that presented in this paper. Our current analysis for Siple Dome dates the same ash layer at 665 ± 30 years. The agreement between Taylor Dome and Siple Dome shows that our compaction analysis is self-consistent between these two different glaciological regimes.

3.8 Conclusions

We have evaluated 2 different methods for measuring vertical strain in the firn. Both have strengths and weaknesses. An important limitation to both methods appears to be the metal marker bands that are tracked over time, which are difficult to install and might be moved by the measuring tool. A future direction for vertical-strain measurement should be to track natural features in the borehole wall instead of artificial markers.

A density profile derived from our vertical strain measurement matches well with measured values, under a range of acceptable accumulation rates. Our derived depth-age relationship is consistently 10-15% younger than depth-age scales derived from layer counting. Changing our long-term average accumulation rate by approximately 10-15% would bring the depth-age profile in-line with those of other investigators, but our corresponding density profile then fails to match measured values. This contradiction may point to the possibility of transient behavior at Siple Dome on the $\approx$700 year time scale represented by the upper 100 meters.

Chapter 4

VERTICAL STRAIN MEASUREMENTS IN FIRN USING BOREHOLE OPTICAL STRATIGRAPHY

This chapter is a manuscript in preparation under the same title for submission to *Journal of Glaciology* with co-author Edwin D. Waddington, who helped guide my research.

4.1 Summary

We have developed Borehole Optical Stratigraphy, a technique in which we use a borehole video camera and post-processing software to make a record of the optical brightness as a function of depth in polar firn. To measure vertical strain, we note the positions of optical features on the borehole wall detected by an initial "baseline" log. We track the displacements of these features in subsequent logs. The result provides a measurement of the relative vertical motion of the firn over the survey period. We used this system at Summit, Greenland to make an estimate of the depth-distribution of firn compaction experienced in a borehole over a 70 day period.

4.2 Introduction

Detailed measurements of vertical strain in the firn have been made in the past using several techniques (Hamilton and Whillans, 1996; Hawley and others, 2002; Paterson and others, 1977; Raymond and others, 1994; Elsberg and others, 2004). In polar firn, measurements of vertical strain can add valuable information to a glaciological field program. Such measurements can provide insight into the mechanics of firn compaction by constraining the actual rates of compaction, and they can be used to assign a depth-age relationship to the shallow sections of an ice core.

Altimetry from aircraft or spacecraft can determine the surface height of an ice sheet, and mass balance can be estimated from changes in this height. However, this height change involves many factors, from isostatic rebound, to accumulation variability, to firn compaction. In-situ measurements of densification can also help in the measurement of mass balance by radar or laser altimetry by constraining the motion of the surface due to firn compaction, which could have a seasonal cycle (Zwally and Li, 2002).

In the past, detailed profiles of vertical strain in boreholes required the placement of artificial markers in the firn, which were sometimes time-consuming and difficult to place, and occasionally were displaced by the measuring tool (Hawley and others, 2005). With the development of Borehole Optical Stratigraphy (BOS, Hawley and others, 2003), we have overcome this limitation to produce a technique that is detailed, accurate, fast, and easy to implement in the field. A measurement of vertical strain using BOS tracks the natural variations in density and grain size in the firn, which produce optical variations recorded by the borehole camera.

4.3 Borehole Optical Stratigraphy

4.3.1 Overview

Borehole Optical Stratigraphy is a borehole logging method that uses a video camera and image processing to measure the relative brightness of the wall of a borehole. In this way, we can obtain similar information in-situ to that which visual stratigraphers obtain from a core. Our vertical strain technique exploits the fact that the BOS log of a borehole contains distinctive features that can be identified and tracked as they move down in the firn column in subsequent logs.

4.3.2 Field instrumentation

Borehole preparation

The borehole to be used for a BOS vertical strain study can be a dry borehole to any depth, although in most locations a dry hole will not stay open if it is too deep. The hole should be drilled with an electro-mechanical drill, to keep the diameter variation to a minimum. The hole must not be fully cased, so that the camera can see the details of the firn in the borehole walls. A casing is desirable to minimize the damage to the top of the borehole from repeatedly raising and lowering the camera. The casing should be short and supported with a board and riser-clamps on the surface so that it does not affect compaction. Our typical installation is sketched in Figure 4.1.

Camera

The down-hole camera is a downward-looking, wide-angle Geovision jr.^{tm} borehole camera from Marks Products of Richmond, VA. The camera has a CCD sensor and provides analog (NTSC) video. Illumination is provided by a set of white LEDs arranged in a circle around the CCD. The camera is supported in the hole by a 3-conductor flat cable which carries the both video signal and camera power. At the surface, the cable runs over a pulley and down to a motorized winch that raises and lowers the camera smoothly. The video signal exits the cable spool via slip-rings and then enters the video-overlay unit described below.

Depth measurement

Depth is measured using the pulley at the top of the borehole. An optical encoder is mounted to the shaft of the pulley, and sends 1000 pulses per turn of the pulley. The encoder sends the pulses as square waves on 2 channels which are 90 degrees out of phase from one another, a scheme known as quadrature encoding. Using a simple state engine, a quadrature decoder can determine the direction of rotation of the pulley from the relative phase between the 2 channels. The circumference of the pulley is 0.3 meters, resulting in a depth resolution of 0.0003 meters. The signal from the encoder is routed to the depth-counter/video-overlay unit.

Counter and overlay electronics

The depth-counter and video-overlay unit is composed of a video-overlay circuit, a depth-counting circuit, and a microcontroller. The depth-counting circuit receives the quadrature pulse signal from the encoder, decodes it and feeds it into a count register in the microcontroller. The microcontroller converts the depth to human-readable ASCII characters and

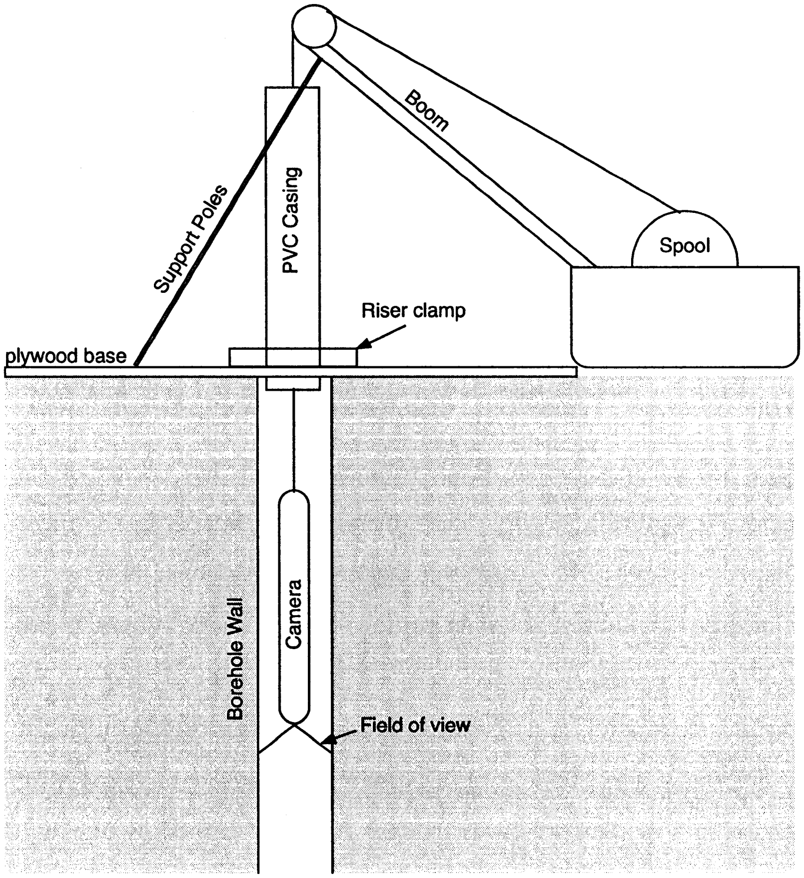

Figure 4.1: Setup of the system

sends it to the video overlay circuit, which combines the text with the NTSC video signal, placing the depth on the upper left corner of the field of view.

The combined signal is then routed to a DV camcorder, which also serves as a field monitor for the down-hole camera. A block diagram of the system is shown in Figure 4.2.

4.3.3 Data reduction

Video capture

The raw digital video signal is captured using an IEEE 1394 interface to a computer using commercial video-editing software, and an image mask is applied to the frame, selecting an annulus of pixels around the borehole wall. This ring represents a small horizontal slice of the borehole over which we will average the returned intensity. After masking, the motion picture is broken down into its component frames (at the DV standard frame rate of 29.97 fps), and each frame is treated individually. A typical frame is shown before and after masking in Figure 4.3.

Optical character recognition

For each frame, our in-house software reads the depth from the upper left corner of the frame using Optical Character Recognition (OCR). The software then calculates the mean value of the remaining annulus of pixels. The resulting depth-intensity series is what we refer to as a BOS profile. Figure 4.4 shows one such profile, from a shallow borehole at Summit, Greenland.

In practice, the OCR routine occasionally mistakes one character for another, resulting in depth errors. Usually these errors are easy to identify because we can reasonably expect the depth series to be continuous with a relatively constant slope. An error in reading one digit will cause a discontinuity in the depth record proportional to the logarithm of the decimal place in the number where the OCR routine erred. The sections that contain such erroneous depths can then be corrected by adding or subtracting digits until the discontinuity in the depth record is eliminated. Finally, for the correlation procedure described below, we low-pass filter the data, to eliminate the possibility of attempting to correlate small fluctuations

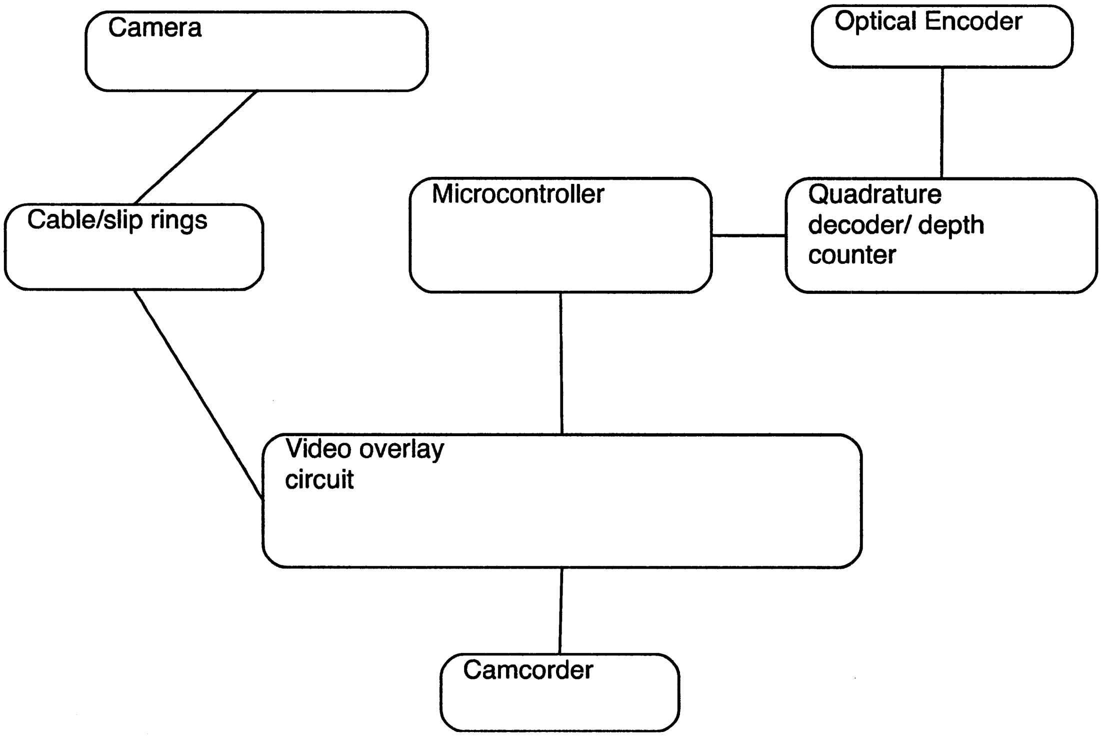

Figure 4.2: Block diagram of the Borehole Optical Stratigraphy System

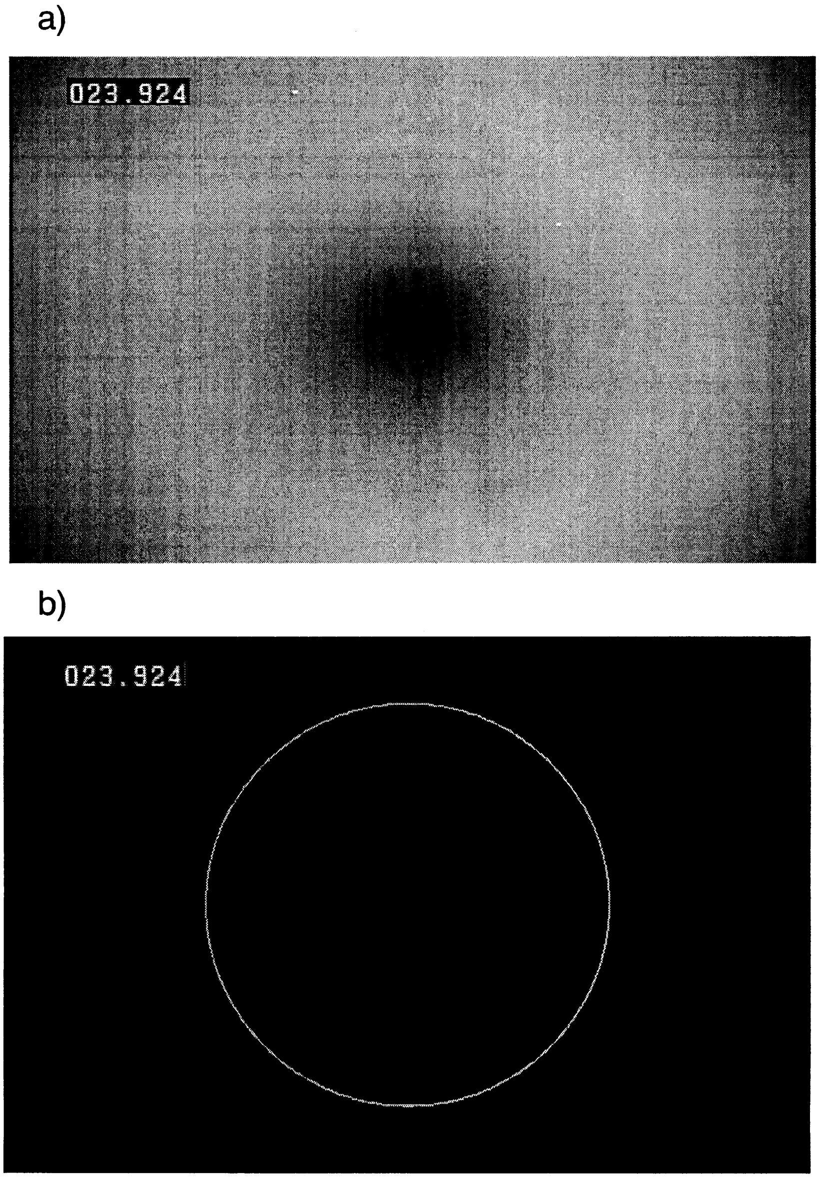

Figure 4.3: Sample frames of the borehole video. Panel a): the raw video log, the camera is looking straight down the borehole. Centralizers hold the camera in middle of the borehole. Panel b): The same frame after initial processing. We have masked out all but a small annulus around the borehole wall. Subsequent steps in the process are to find the average brightness of these pixels, and to read the depth for the image using Optical Character Recognition.

that might result from noise in the video log. We use 5 cm as a cut-off length-scale for filtering because we can visually identify repeatable features above this scale.

4.4 Determining Vertical Strain

4.4.1 Co-registration of independent logs

Once we have two BOS logs of the same borehole taken at different times, we can determine the vertical strain that has taken place in the time between the two logs. The greatest source of error in the depth measurement arises from the human element of setting the zero depth of the camera at the beginning and end of the log. To avoid this issue, we first use cross-correlation to align the two logs near the bottom of the hole.

4.4.2 Windowed correlation

We now cross-correlate the 2 logs in 1 meter windows. We largely follow the approach described by Scambos and others (1992) for 2-d image correlation. Our situation is simpler because we have only one dimension. For each section of the log, we begin by cross-correlating the section (the reference section) with a larger window on the original log (the search area). We then re-align the log with the offset producing the maximum correlation. To determine a first estimate of total strain profile, we examine the correlation coefficients obtained in the cross-correlation process. We discard any matches that result in a correlation coefficient < 0.9. The remaining points make up the basis of our initial estimate. Each point represents a depth and a total motion relative to the deepest detected features. We then approximate the strain function by fitting a quadratic to these points. Once we have a first estimate of the strain function, we repeat the cross-correlation procedure, this time using 0.2 meter windows. Again examining the correlation coefficients, we now discard any matches that result in a correlation coefficient < 0.99. The total displacement and depth at these matched points makes up our detailed strain profile.

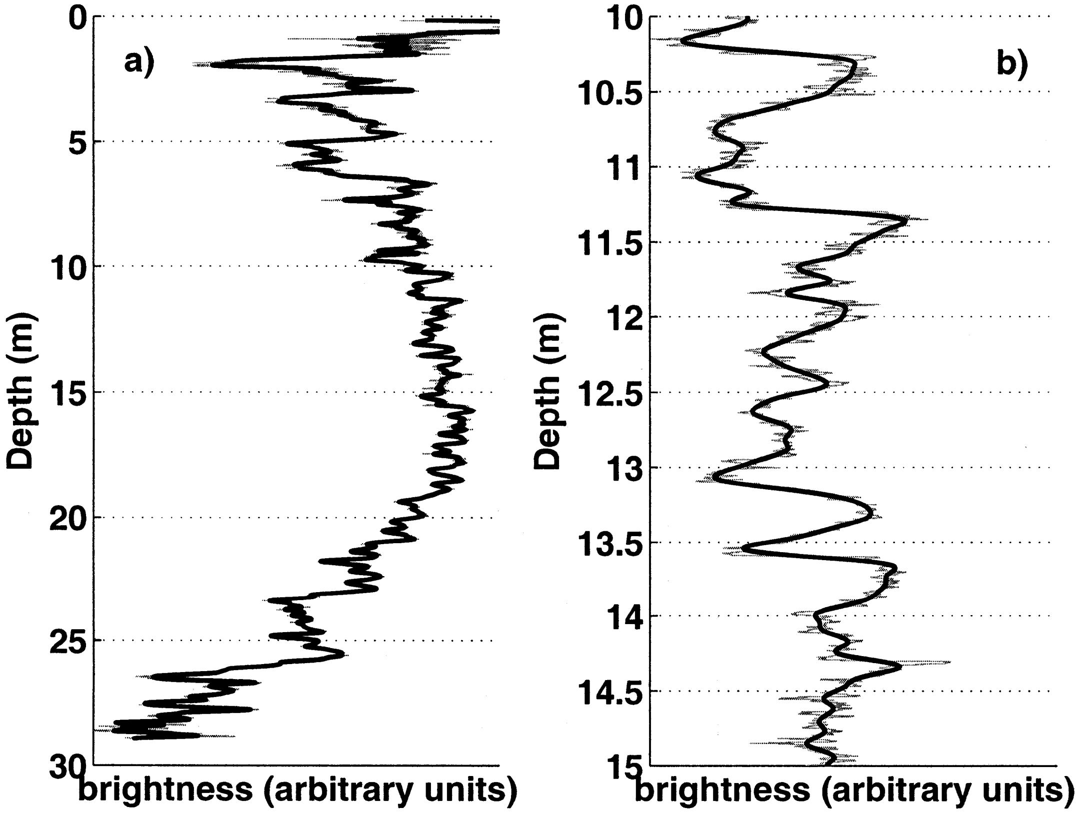

Figure 4.4: Panel a): The complete log of of the "Katie" borehole on June 9, 2004. Panel b): a short section of the same log, enlarged to show the details we will be correlating. The unfiltered log is shown in light grey, and the low-pass-filtered (cutoff ≈ 5cm) log is shown as the solid black line. The filtered log has many distinct features to be correlated.

4.5 Test Case: Greenland Summit

We deployed this system in an array of shallow boreholes at Summit camp, Greenland. The boreholes were drilled with the Ice Core Drilling Services "Prairie dog" electro-mechanical drill. The boreholes are 30 meters deep, covering the shallow region where firn compaction is most rapid. We present here the strain result for two borehole logs taken in the same hole approximately two months apart. The first log was taken on June 9, 2004, and the second was taken on August 17, 2004. Figure 4.4 shows the June 9 log in its entirety, along with the filtered data used for the correlation. To illustrate the process of "unstraining" the August 17 log, figure 4.5 shows short windows (shallow and deep) of the two filtered logs side-by-side, before and after the cross-correlation process.

The initial estimate and final strain profiles are shown in figure 4.6. In section 4.6.1 below, we use the value of our first estimate at the surface to check our measurement against a first-order estimate of compression based on mean annual accumulation and the assumption of steady state densification.

4.6 Discussion

4.6.1 Expected compaction

At this low-divergence location, in steady state, the amount of water that falls as snow on the surface of the ice sheet must pass through an imaginary plane at depth corresponding to the bottom of the borehole, following mass continuity. Specifically, if $\dot{b}$ is the average accumulation rate in ice equivalent units and ρ_{bot} is the density at the bottom of the borehole, the bottom of our borehole is moving down in the ice sheet (mostly due to continued firn compaction) at a rate of $\dot{b}\frac{\rho_{ice}}{\rho_{bot}}$. Similarly, the top of our borehole is moving down in the ice sheet at $\dot{b}\frac{\rho_{ice}}{\rho_{surf}}$ with ρ_{surf} the surface density. The difference between these two rates is the rate of compression of the firn column v_{fc}. Thus,

$$v_{fc} = \dot{b}\left(\frac{\rho_{ice}}{\rho_{bot}} - \frac{\rho_{ice}}{\rho_{surf}}\right). \tag{4.1}$$

The density at the surface at this site is ≈ 0.3 g cm^{-3}, and at the bottom of the borehole reaches ≈ 0.6 g cm^{-3} (unpublished field data, G. Lamorey and R. Hawley 2004). The

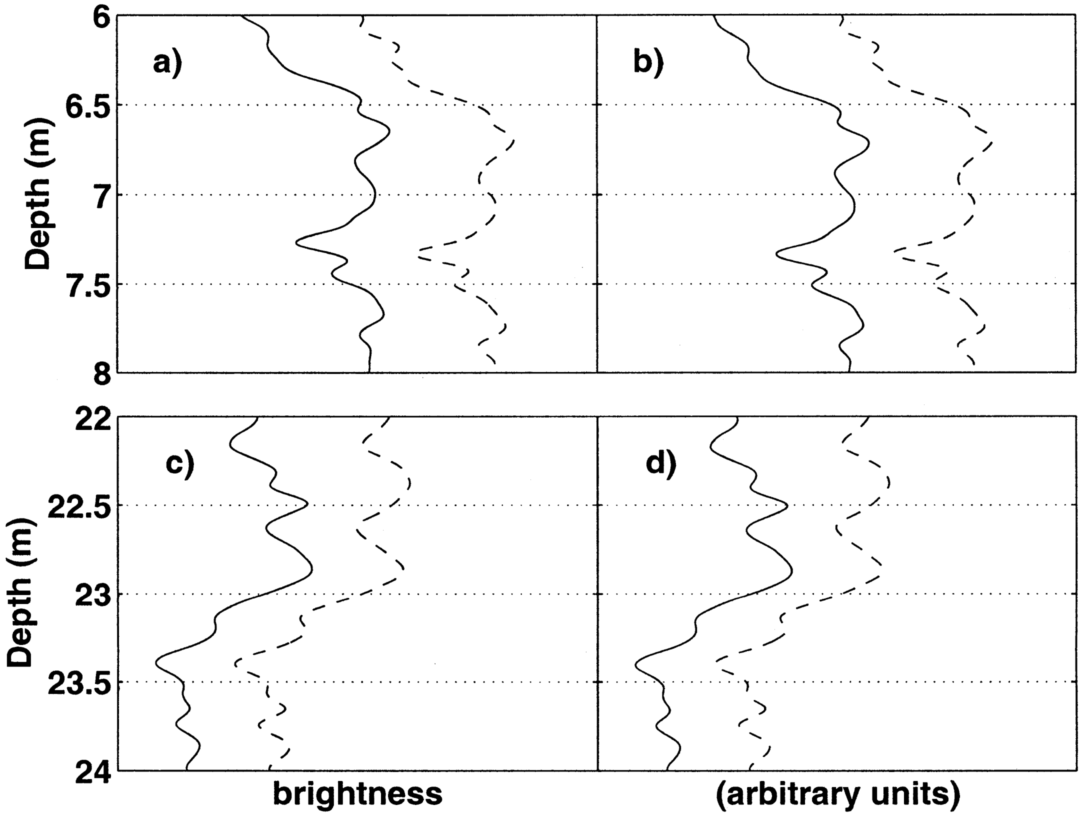

Figure 4.5: The 2 logs before and after "unstraining" the second log. The first log is shown as a dashed line and the second as the solid line. Panel a): A shallow section showing the two logs. Note the slight offset of the features. Panel b): After "unstraining", the features are now aligned. Panel c): A deeper section of the logs. The offset is much smaller here. Panel d): After "unstraining". Here the change is more subtle.

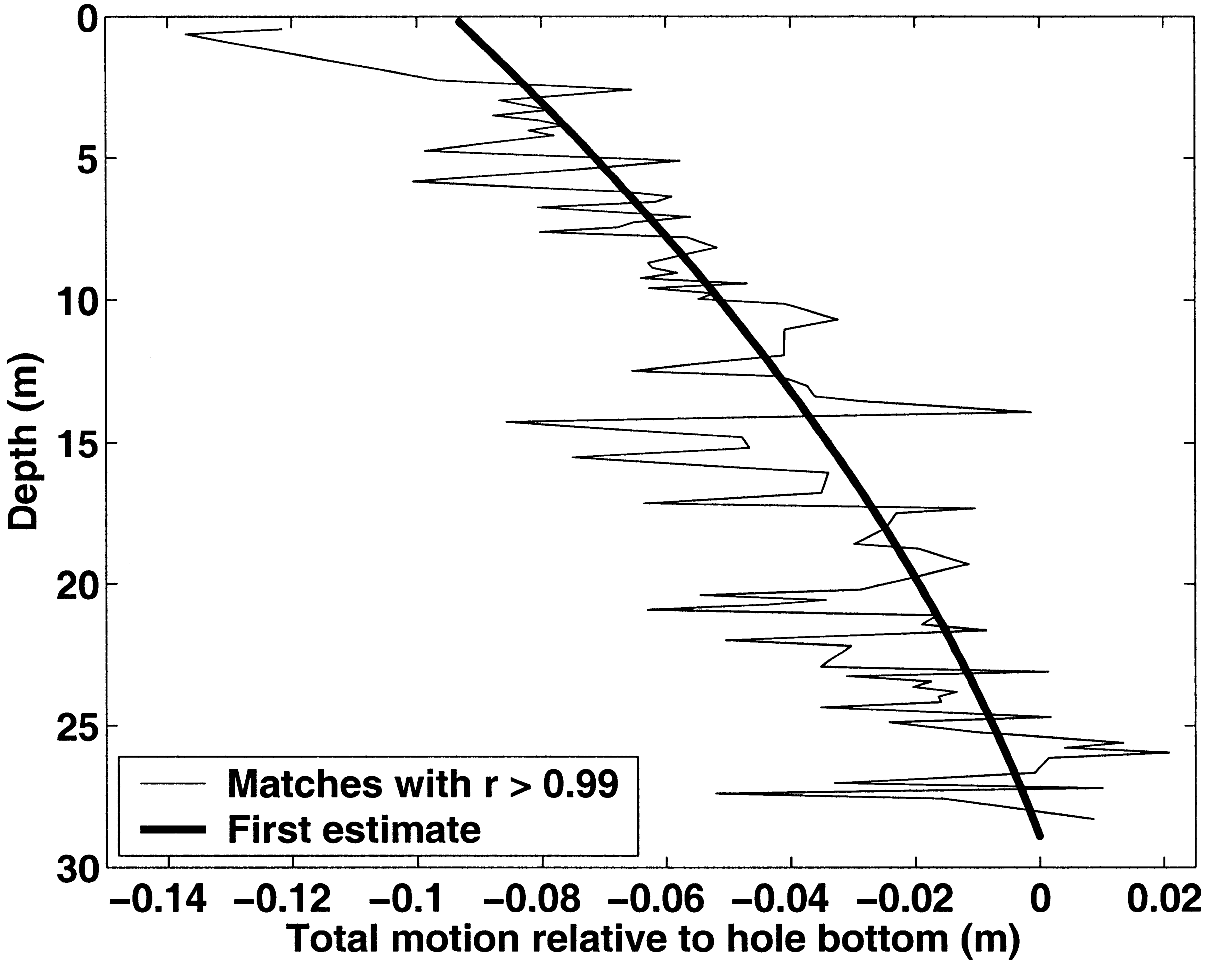

Figure 4.6: The final strain profile. The fine line shows depth-offset pairs that resulted in a correlation of > 0.99. The heavy line is our first estimate of the strain profile.

accumulation rate $\dot{b}$ is ≈ 0.25 m a^{-1} ice-equivalent (Meese and others, 1994). Using these values in equation 4.1, we get $v_{fc} = -0.38$ m a^{-1} .

To find the expected shortening of our borehole over the survey period of 70 days, we multiply this by a factor of $70/365 = 0.192$, finally arriving at $v_{fc}(70\text{days}) = -0.38 \times 0.192 = -0.073$. So our expected total shortening over the survey period is ≈ 0.073 meters. Our first estimate from our measurement, shown in in figure 4.6 is ≈ 0.093 meters, close to what we expect from our order-of-magnitude estimate.

4.6.2 Variability in compaction

The thin line in figure 4.6 shows considerable excursions from the initial estimate (the heavy line). The magnitude of these excursions is larger than what would be expected from inaccuracies in the depth counting system, and they are not characterized by periodicities that might be expected if they were caused by a pulley with an off-center axis- these variations may be evidence of differential compaction of the firn. Although a full discussion of firn compaction is beyond the scope of this paper, differential compaction could have many causes. Zwally and Li (2002) modeled firn densification and concluded that snow deposited in late spring and summer could compact faster than snow deposited in late fall and winter. In the shallow regions of our survey, temperature differences in the firn could drive different densification rates.

4.7 Conclusions

We have successfully measured vertical motion in polar firn using the new technique of Borehole Optical Stratigraphy. This method is fast and easy to implement in the field, and with simple analysis can provide a measure of the vertical motion in the firn as a result of firn compaction. Our detailed record of compaction shows differences in the rate of densification rate as a function of depth. This differential compaction could have many causes. With further study and frequent observations, we hope to characterize these spatial, as well as possibly temporal, variations in firn compaction.

Chapter 5

ANNUAL LAYERS IN POLAR FIRN DETECTED WITH BOREHOLE OPTICAL STRATIGRAPHY

This chapter was published under the same title in *Geophysical Research Letters* **30**(15) with co-authors Edwin D. Waddington, Richard B. Alley, and Kendrick C. Taylor. It was reviewed and accepted without specific comments by anonymous reviewers. The specific contributions of my co-authors were as follows: Ed Waddington initiated the Siple Dome project and helped develop BOS, helped guide my research, and edited the manuscript. Richard Alley and Ken Taylor provided layer-counted depth-age profiles (using visual stratigraphy and electrical stratigraphy, respectively) that I use to validate my results.

5.1 Summary

We have developed a system called Borehole Optical Stratigraphy which can detect annual layers in boreholes in polar firn. Borehole Optical Stratigraphy consists of a downhole camera package and post-processing routines, which allow us to measure the intensity of light emitted from an on-board source and returned from the borehole wall. We manually identify the annual layers in this optical signal. We used this system at Siple Dome, Antarctica, in the 2001-2002 austral summer season. Our results agree well with counts of annual layers detected with two different methods in an ice core recovered 50 meters from our borehole.

5.2 Introduction

Determining the age of ice at a given depth is fundamental to ice-core research. Many different methods for dating ice cores exist (eg. Hawley and others, 2002; Alley and others, 1997; Meese and others, 1997; Steig and others, 1998). Of these, the most detailed record can be obtained by counting annual horizons preserved in the stratigraphy of the ice. These layers can be detected in an ice core by electrical, chemical, isotopic, or physical means (Meese and others, 1997). We have developed Borehole Optical Stratigraphy, a system that can optically detect annual layers directly on the walls of a borehole. There are significant advantages of such a system; a preliminary depth-age scale can be determined with a few hours of processing in the field, and no core is needed so the procedure can be used in holes drilled with faster non-coring drills as part of site selection for a coring project. We have used this system to date the firn at Siple Dome, Antarctica. Our Borehole Optical Stratigraphy depth-age scale agrees well with those produced by visual observation and Electrical Conductivity Measurement (ECM) analysis of annual layers in a nearby ice core.

5.3 Borehole Optical Stratigraphy

5.3.1 Field measurements

Our Borehole Optical Stratigraphy field system consists of a downhole camera connected to a digital video recorder at the surface. The downhole package is a downward-looking, wide-angle commercial video camera with integrated Light Emitting Diode (LED) scene-illumination lights. Since the camera looks down and has a wide field of view, the entire circumference of the borehole wall can be seen. The depth of the camera is measured by a rotary encoder attached to the sheave wheel over which the cable runs down into the hole; the measured depth is displayed in the video field of view. With a motorized winch, we lower the camera at a constant speed for the entire log. Since the digital video standard takes 29.97 frames per second, we can vary our logging speed to control the depth interval between frames. Typically we collect one image every 1-2 mm, and thus a 100 m borehole takes about 30-60 minutes to log.

5.3.2 Post-processing

The resulting log is a recording of the borehole wall covering the entire depth of the hole, with depth information incorporated. To detect annual layers, we process this motion picture to produce an optical "brightness" value for each depth. To get a brightness for each frame of the video, we take an average of the pixel values in an annulus around the borehole wall. The depth is read from the image using optical-character-recognition software. The result is a brightness vs. depth record. A representative short section of one such log is shown in

Figure 5.1.

5.3.3 Source of brightness variations

The variations in brightness seen in Figure 5.1 most likely result from the same subtle differences in grain size, bubble size, and density that allow the visual identification of annual layers in ice cores. Repeat logs of the same hole (Figure 5.2, panel a) show the same features from one log to the next. "Blank" tests (logs with a hood placed over the camera and light source, isolating them from the environment) indicate that the source light on the camera is very stable and could not be responsible for the variations we see. Tests of the distribution of brightness around the annulus (Figure 5.2, panel b) show that we are seeing near-horizontal layers and not isolated bright spots in the wall.

5.4 Visual Stratigraphy

Analysis of visible structures in ice cores is one of the oldest techniques in ice-core studies. Many different structures can be visually identified in a core. Annual-layer counting by visual means is based on differences in appearance of summer and winter snow. In shallow firn at Siple Dome, the most prominent annual stratigraphic marker is the "depth hoar / wind slab couplet", consisting of course-grained depth hoar, formed in the summer when strong temperature gradients promote grain growth in the snowpack, overlain by a fine grained, wind-packed layer formed in the winter (Alley, 1988; Alley and others, 1997). Visual stratigraphers also note occasional melt layers in cores. Some melt layers were identified at Siple Dome, but are infrequent and were indistinguishable in the borehole log. Dust concentration has been measured with optical methods, both in cores and in deeper ice (Ram and Koening, 1997; Bay and others, 2003). We did not see dust layers in our logs at Siple Dome, nor did visual examination of the core identify major visible dusty horizons in the depth interval of the borehole observations. Mechanical marks left on the borehole walls by the drill could potentially affect our measurement, by changing the angle of incidence and thus the scattering properties of the wall. In practice, a gouge in the wall from the drill is likely to be more striking, with a sharply defined edge, than the more smoothly varying

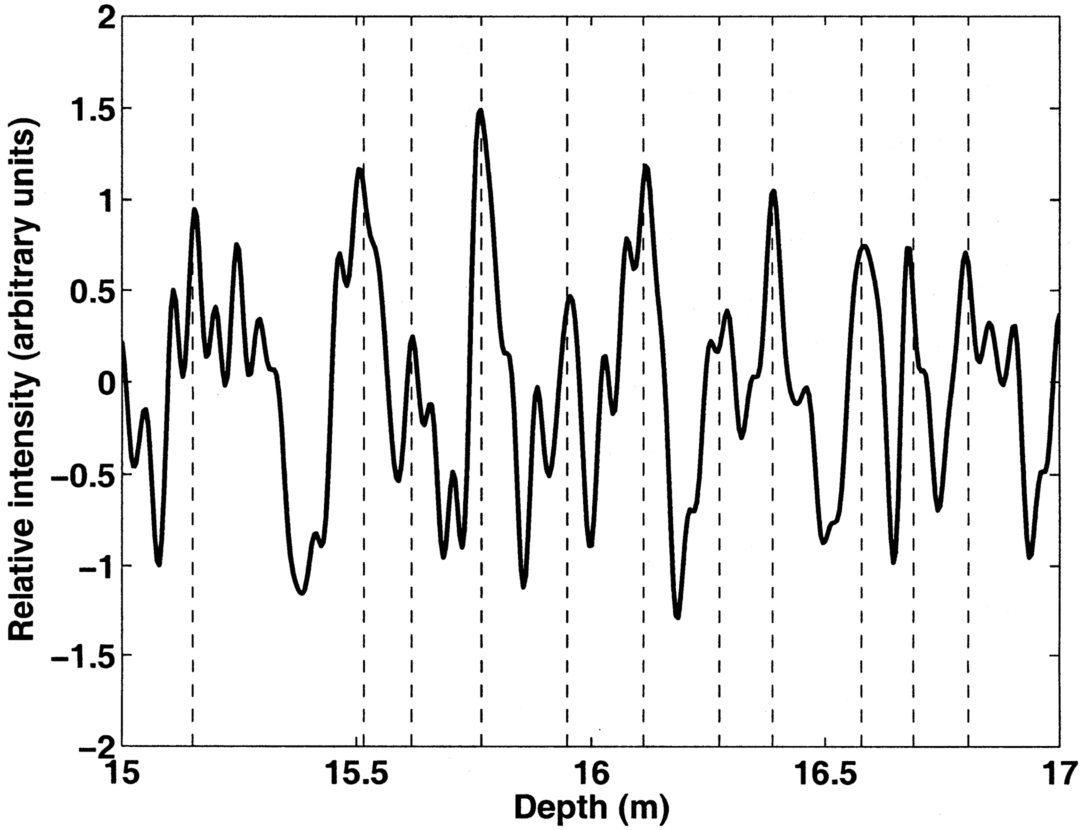

Figure 5.1: Band-pass filtered Borehole Optical Stratigraphy signal (heavy solid line) and the depths of "Annual Layer" picks (dashed lines). The band-pass filter passed fluctuations of 1 to 50 cm wavelength. Peaks in brightness were chosen as the "Annual" markers.

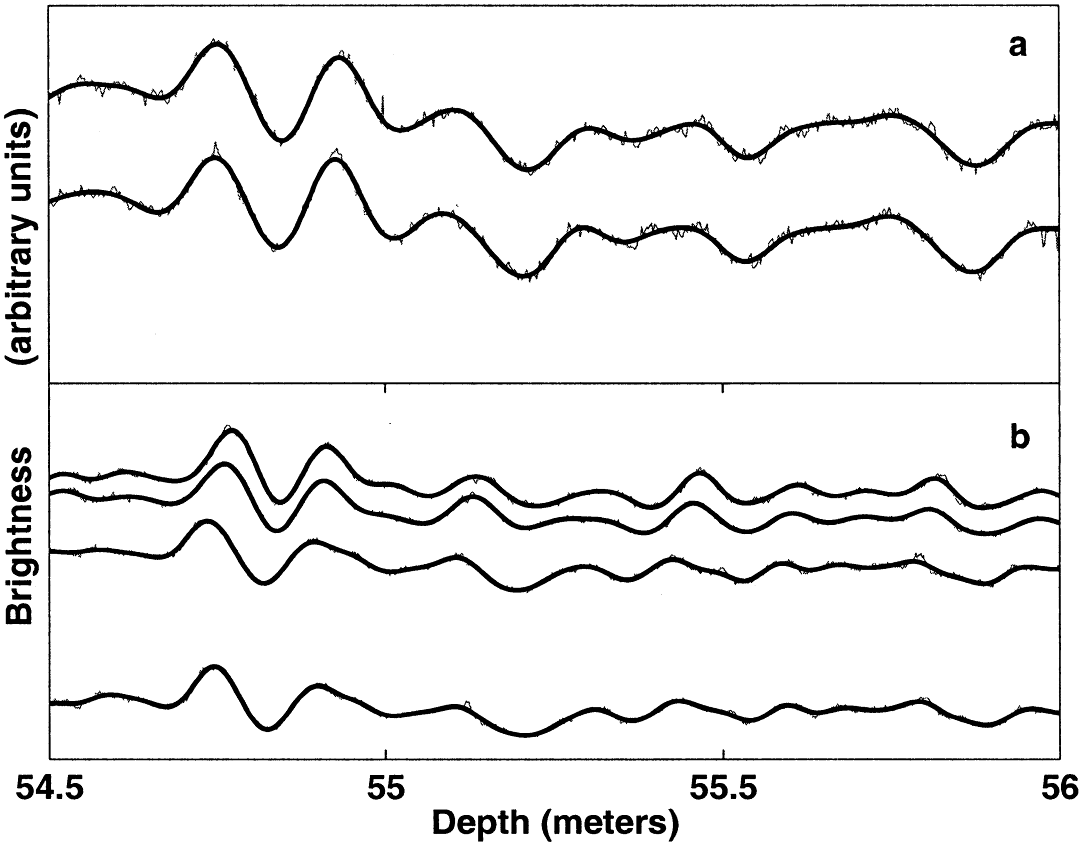

Figure 5.2: Panel a: Repeat logs of the same hole, taken one day apart. Clearly we are seeing the same features. Panel b: A third log of the same hole, with the annulus divided into four quadrants, each averaged and plotted separately. The correlation indicates that the features are near-horizontal stratigraphic layers in the walls of the borehole.

features we see in the log. Presumably such marks would also be visible and identifiable in the raw log footage, and no such marks were seen. Although we cannot exclude the possibility that "drill scarring" could affect our signal, these characteristics indicate that any artifacts caused by drilling are likely to be small.

5.5 Analysis

Once the Borehole Optical Stratigraphy log has been processed and a brightness profile produced, we must identify the annual layers. One option is to visually examine the record and hand pick peaks or troughs. We suggest that peaks in brightness correspond to zones of fine-grained snow or firn that cause increased backscatter of light to our instrument (Wiscombe and Warren, 1980). These zones are the "wind-slab" component of the annual "depth hoar / wind slab couplet" that forms the basis for annual layer stratigraphy. Our approach is to first band-pass filter the data, to eliminate oscillations shorter than 1 cm or longer than 50 cm, and then to visually pick the significant peaks. In practice, our continuous log was broken up into a series of ≈5-meter sections because there were metal markers in the hole at these intervals (see Hawley and others (2002) and Hawley and others (2005) for a discussion of these markers). We interpolated layers across the ≈50 cm data gaps left by the metal markers. The resulting depth-age scale is shown in Figure 5.3. Also shown for comparison are 2 other depth-age scales determined by annual-layer counting in the SDM-A core, ≈50 meters away. The Pennsylvania State University (PSU) team visually examined the core and identified annual horizons. The Desert Research Institute (DRI) team used a computer algorithm (Taylor and others, 2002) to identify annual cycles in electrical conductivity records on the core. All agree within ≈10 percent.

5.6 Discussion

The identification of annual layers is generally considered to be difficult, and there are often differences between observers for a given section of core. Sometimes the same observer can obtain different layer counts on the same section of core when counting on different days. Accuracy of annual layer counting by visual means depends on accumulation rate and other

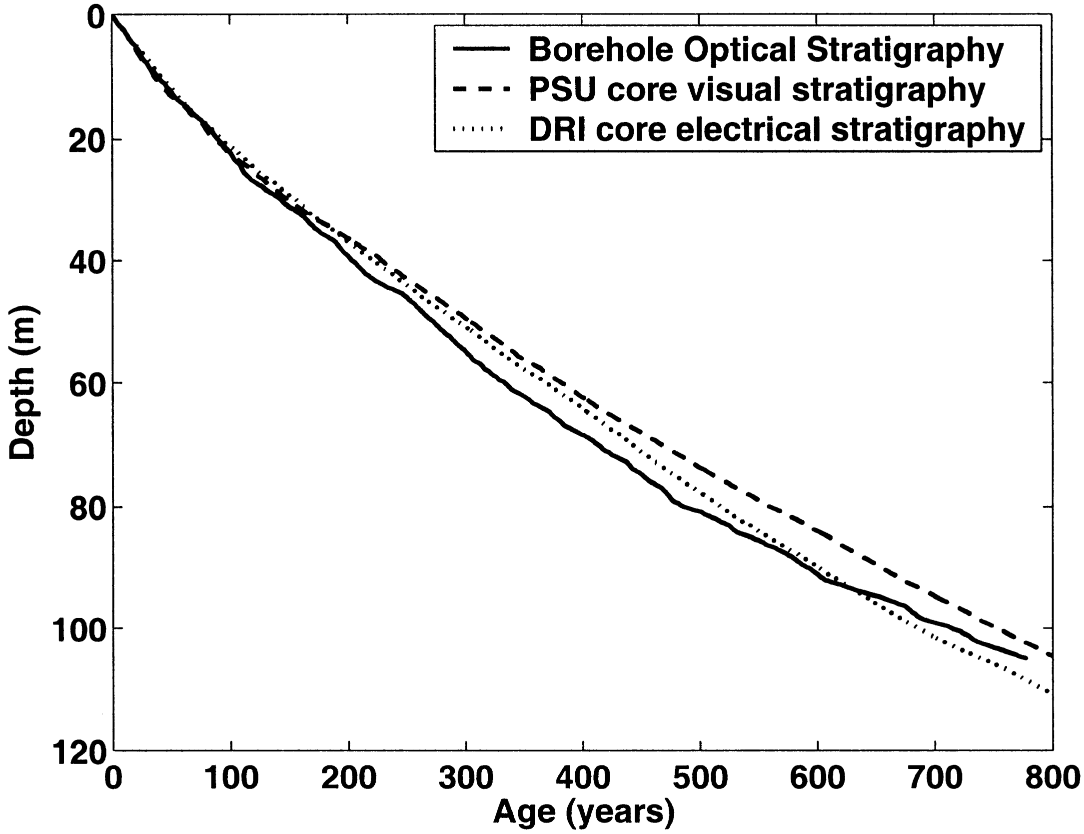

Figure 5.3: Depth-age profiles at Siple Dome from annual-layer counting. The solid line is from layers manually counted with Borehole Optical Stratigraphy. The dashed line is from layers in a nearby core counted visually by PSU. The dotted line is also from the nearby core, but used the DRI autopicker to count layers in the ECM record.

factors, with errors ranging from ≤1% to many percent or more (Alley and others, 1997; Taylor and others, 2002). With its relatively low accumulation rate, Siple Dome is unlikely to yield ≤1% accuracy, as witnessed by the differences between the PSU and DRI curves in Figure 5.3. Owing to spatial variability in formation of annual layers (Alley, 1988), and to the possibility that slight core loss during recovery affected subsequent observations, we do not expect exact correspondence between layers identified visually or in other ways on the core, and layers observed in a borehole ≈50 m away. As an alternative measure of our success in detecting annual layers, Figure 5.4 compares the thicknesses of annual layers detected by the three methods. Panel a shows that manually picked layers from Borehole Optical Stratigraphy match the smoothed layer thickness vs. depth curves from visual stratigraphy and electrical stratigraphy well. Near the bottom of the profile Borehole Optical Stratigraphy appears to contain slightly thinner layers on average than the other methods, and this effect can be seen in the accompanying histograms. If this is anything more than a difference between observers, it could result from decreasing contrast at greater depths, which makes individual layers more difficult to identify. A future logging tool might overcome this limitation by having an adjustable light source to improve the signal strength at greater depths. The histograms show that although the PSU visual stratigraphy has the lowest standard deviation, the range of layer thicknesses is similar among all three methods. This gives us greater confidence in our ability to detect annual layers.

5.7 Conclusions

Borehole Optical Stratigraphy can be used to quickly determine a depth-age relationship for polar firn. Our depth-age relationship derived by counting annual layers on a borehole wall is very close to those derived by other observers counting layers in a nearby ice core. The unique ability to detect annual layers in a borehole makes Borehole Optical Stratigraphy a valuable tool for ice-sheet dynamics and ice-core paleoclimate studies. Using Borehole Optical Stratigraphy for annual-layer detection in the future could allow rapid characterization of large areas during ice-core site selection. For example, by placing absolute dates on the layers detected by Ground Penetrating Radar, we could infer temporal and spatial

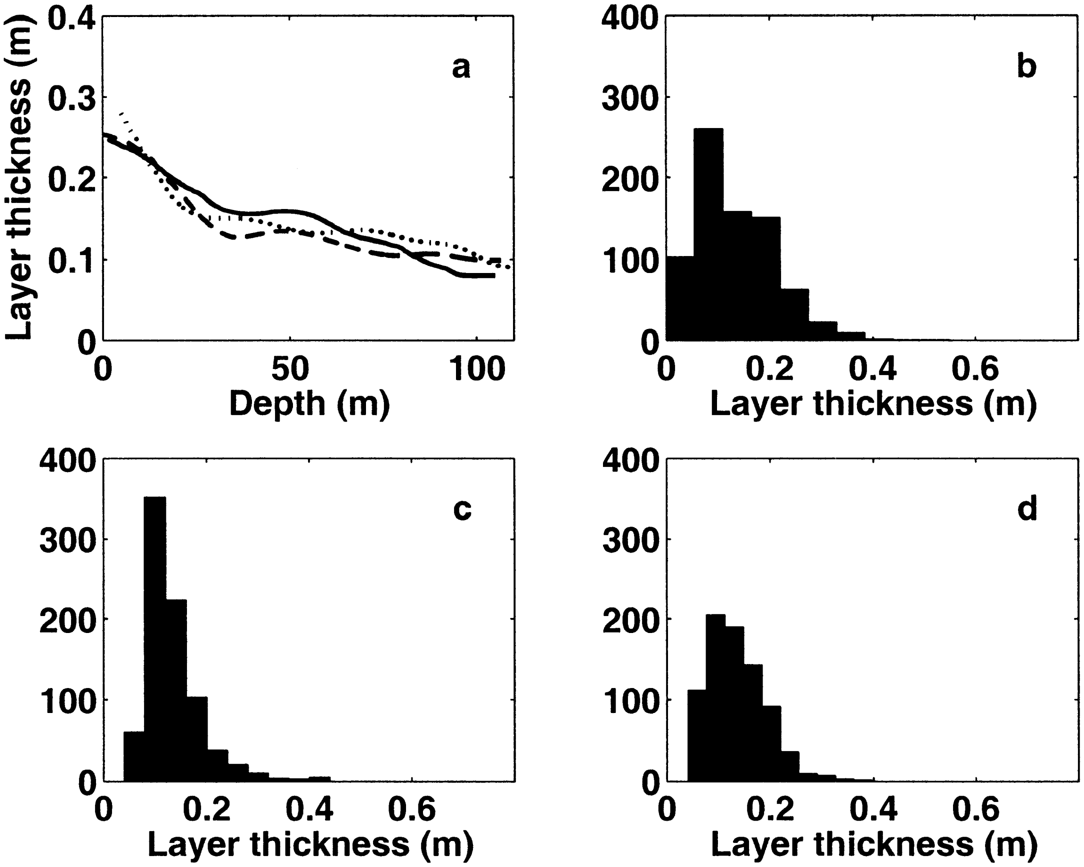

Figure 5.4: Comparisons between layer-counting methods. Panel a: smoothed annual layer thickness vs depth showing reasonable agreement among three methods of determining annual layers: Borehole Optical Stratigraphy (Solid curve), visual stratigraphy on the core (dashed curve), and electrical stratigraphy on the core (dotted curve). Panels b-d: histograms of the layer thickness determined by Borehole Optical Stratigraphy, PSU visual stratigraphy, and DRI electrical stratigraphy, respectively.

variability in accumulation rate over a large region.

Chapter 6

BOREHOLE OPTICAL STRATIGRAPHY AND NEUTRON-SCATTERING DENSITY MEASUREMENTS AT SUMMIT, GREENLAND

This chapter is a manuscript in preparation under the same title for submission to *Journal of Glaciology* with co-author Elizabeth M. Morris. Liz Morris collected and provided the density data, and reviewed the manuscript.

6.1 Summary

We have made side-by-side measurements in several boreholes at Summit, Greenland, using Borehole Optical Stratigraphy (BOS) and Neutron-Scattering density logging techniques. The BOS logs show a high degree of correlation at shallow depths with Neutron Scattering logs taken in the same borehole. This supports the hypothesis that BOS detects changes in density, perhaps through a correlation with grain size, as well as possibly other parameters. The correlation between returned brightness and density decreases with depth and finally becomes negative. This inversion of correlation may be related to changes in densification regime from grain-boundary sliding to pressure sintering.

6.2 Introduction

Analyzing stratigraphy within a snowpack is one of the most fundamental activities in glaciology. It is usually carried out by digging pits, observing visual layering, and conducting simple physical tests on the snow. Stratigraphy is also analyzed in ice cores, using measurements of visible layering, electrical properties, chemistry, and dust concentrations. Visual stratigraphic measurements have been made extensively in snow pits and on cores for many years. Many different types of layers can be observed, from melt layers to dust or ash layers from a nearby (or sometimes distant) volcanic eruption (Alley and others, 1997).

The most readily detectable layering is the "wind-slab/depth-hoar couplet", which forms the basis of annual-layer counting. This couplet is composed of a layer of low-density course-grained "depth-hoar" over-lain by a layer of higher-density, fine-grained "wind-slab". The depth-hoar is formed by thermal-gradient metamorphism in the late summer when strong thermal gradients are present in the upper few decimeters of the snowpack, and the wind-slab is formed by winter deposition of wind-blown snow (Alley, 1988).

Recent advances in borehole techniques make it possible to measure snow and firn stratigraphy in a borehole, with no need for a core or deep snow pits. The "wind-slab/depth-hoar couplet" has been identified with Borehole Optical Stratigraphy (Hawley and others, 2003), and also with the Wallingford neutron probe (Morris and Cooper, 2003). Shallow borehole measurements span the range between snow-pit studies and core analyses, in that they can penetrate far deeper than practical for a snow pit, but they can be performed rapidly in the field with no need to transport core to a laboratory for analysis. Borehole measurements can be repeated to asses in-situ changes of the properties of firn, and provide a continuous, unbroken record.

6.3 Methods

6.3.1 Field Location

Summit camp is a year-round research camp located near the summit of the Greenland ice sheet, at $\approx 72.58^\circ$N, 38.47° W. It is the site of an ice core drilled 3054 meters to bedrock, completed in 1993. The 30-meter borehole used for this work is close to the main camp, approximately 1 km away. The mean-annual temperature at Summit is -31°C and the mean accumulation is ≈ 25 cm a^{-1} (ice equivalent) (Meese and others, 1994; Alley and Woods, 1996).

6.3.2 Field measurements

Borehole Optical Stratigraphy

Borehole Optical Stratigraphy has been developed as a technique for simple and rapid measurement of vertical strain in a borehole. The equipment and processing involved in creating a BOS profile are described in detail in Hawley and Waddington (2005). In essence, the measurement uses a borehole video camera to obtain a video log which contains similar information to that observed by visual stratigraphers on a core. The borehole probe is a downward-looking, wide-angle video camera connected to the surface by a 3-conductor cable which carries both video signal and power. A portable DV camcorder at the top of the hole allows us to view and record the log. The depth of the camera is measured with an optical encoder mounted on the shaft of the pulley over which the cable runs into the hole. This depth is then written in the upper left corner of the video screen. In post-processing, an annulus of pixels around the borehole wall is sampled and the mean intensity of these pixels is recorded. At the same time, the depth is read from the frame using optical character recognition. The end product of the BOS process is a log of intensity vs. depth. Figure 6.1 shows a complete log of the borehole used in this study.

Neutron-scattering density probe

The density probe used for this experiment was a version of the Wallingford soil-moisture probe, adapted for use in measuring snow density as part of an Ice Geophysical Logging System (IGLS). The probe consists of an annular radioactive source of fast neutrons around a cylindrical detector of slow neutrons. Fast neutrons are emitted from the source. As they move through the snow, they lose energy by scattering. The count rate of slow neutrons arriving back at the detector per unit time is related to the density of the snow averaged over a sphere of influence of 15-30 cm radius (depending on density).

An empirical calibration equation (Morris and Cooper, 2003) relates count rate to the density of the surrounding medium, given the borehole diameter and distance from the wall of the borehole (degree of centralization). Errors in the density can arise from deviations from the nominal borehole diameter and deviation from the nominal degree of centralization.

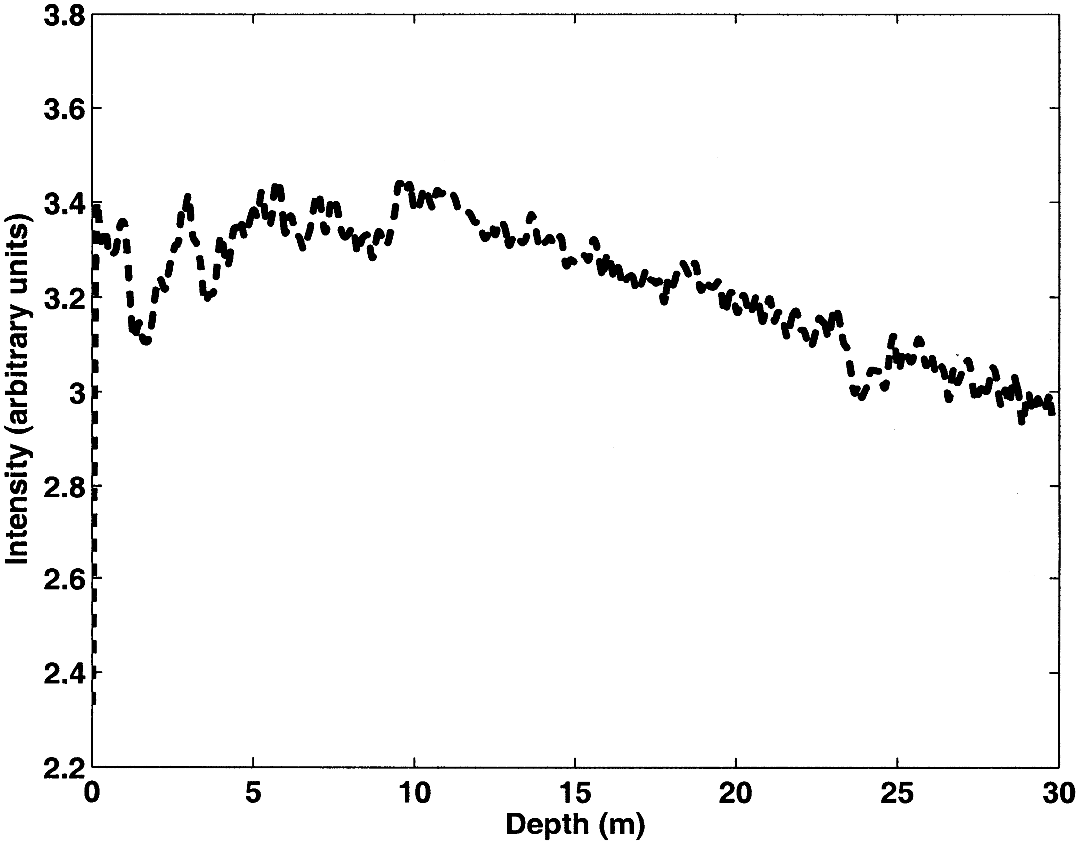

Figure 6.1: The BOS profile.

These errors can be reduced if the actual borehole diameter is measured as a function of depth using calipers and if the neutron probe is held in position, either using a centralizer, or using a spring device to hold it against the wall of the borehole.

The emission of fast neutrons is a random process, so the relative error in the count rate decreases with a lengthened counting period and with increased source strength. Using a radioactive source small enough to be easily manageable in the field, logging speeds of $\approx$ 2 cm min^{-1} are required. The result of an IGLS log is a profile of density averaged over 15-30 cm as a function of depth. Figure 6.2 shows a complete log of the borehole used for this study. Figure 6.3 shows the two logs plotted together to show some of the common features.

6.4 Data Reduction

6.4.1 Differences between depth measurement systems

Since the BOS and IGLS logging systems are independent systems using different methods of depth measurement, a depth calibration is needed in order to compare logs performed with the two systems. The calibration addresses two issues. First, the different systems sample the borehole wall at a point along the tool, and this point has some finite distance from the fiducial mark on the tool where the surface is referenced. Thus a simple constant offset must be added to the depths of one tool to co-register it with the other. Second, the two systems have different measuring units and different pulleys. This second factor requires a linear multiplier of the depth in addition to the offset. The basic form of the transform then is:

$$z^* = mz + b \tag{6.1}$$

where z is the original depth in the BOS log, z^* is the depth to be used for comparison with the density log, and m and b are constants to be determined. To determine m and b, we chose 2 "landmark packets" of features, one near the surface and one around 15 meters, which were of the same shape in each log and were clearly the same features. We varied b to find the maximum correlation between the two logs at the shallow region, and then varied

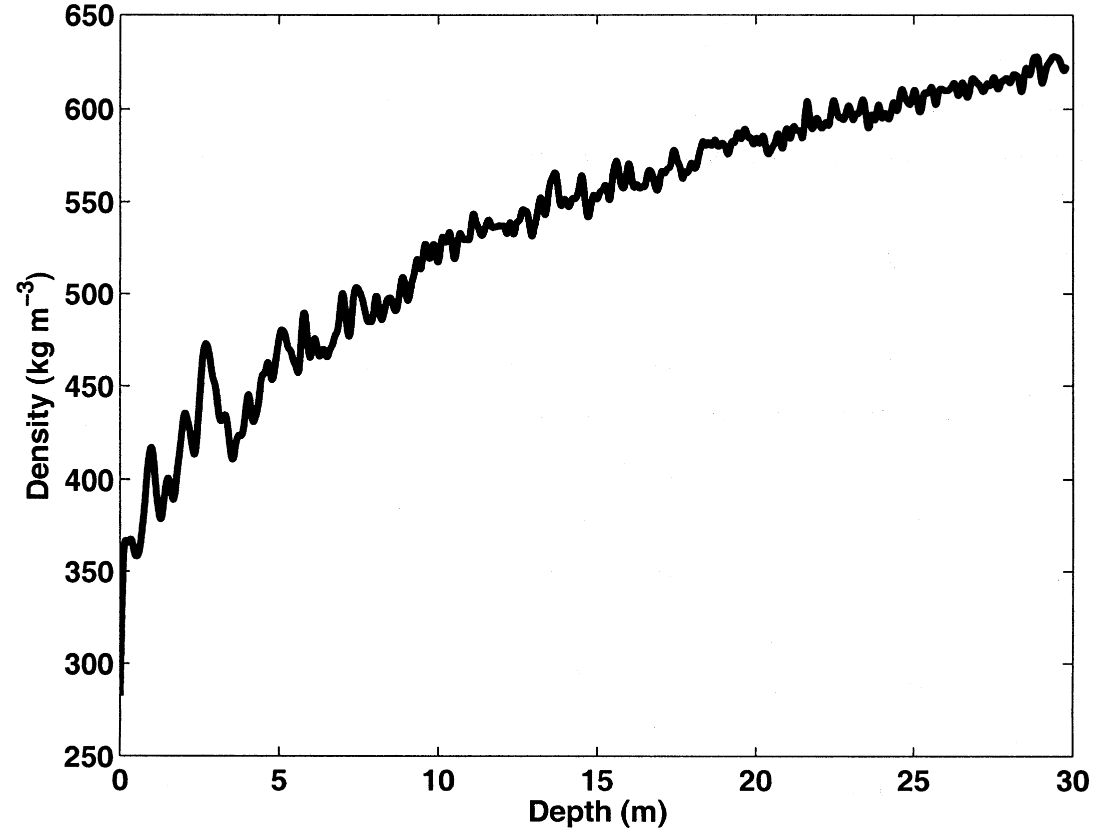

Figure 6.2: The density profile.

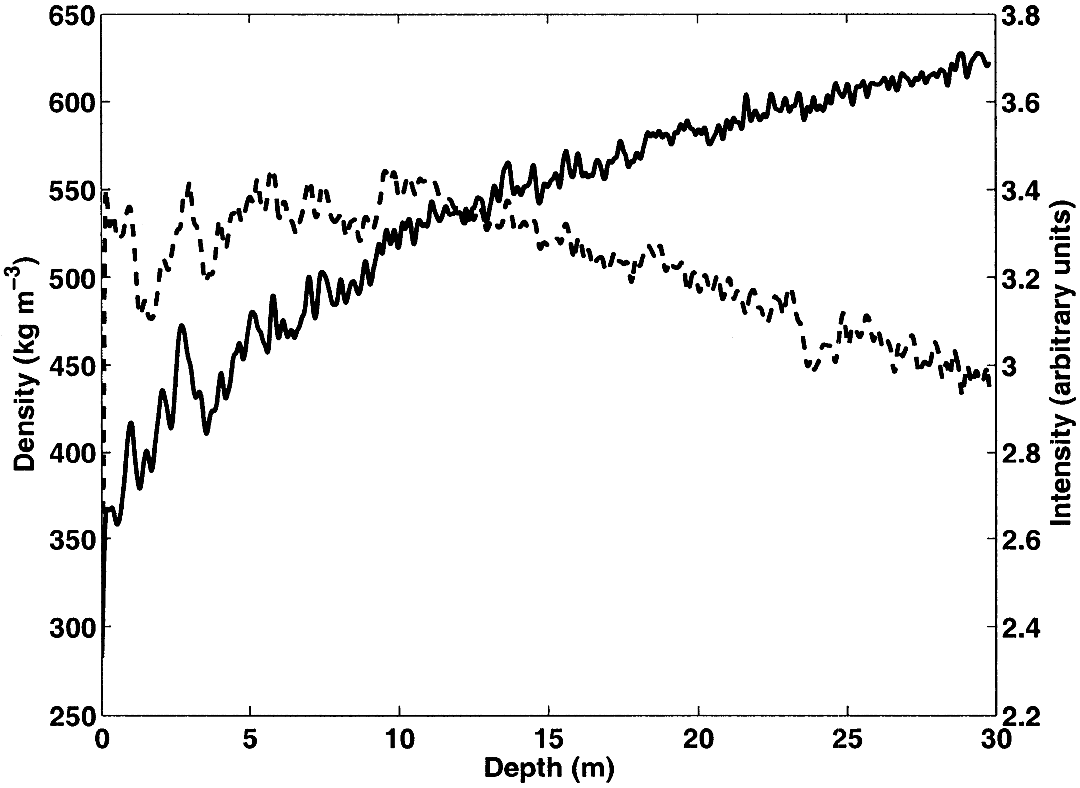

Figure 6.3: The density and optical profiles plotted together. Density is the solid line and intensity is the dashed line. Several features can be seen that are replicated in the 2 logs, particularly in the shallow region.

m to find the maximum correlation between the logs in the deeper region. Our accepted values of m and b were 0.99 and 0.4 m, respectively. Figure 6.4 shows the 2 sets of features we used for this calibration. In this way, we co-register the two logs to the depth scale used by the IGLS.

6.4.2 Filtering and correlation

Since the IGLS samples a sphere roughly 15-30 cm in diameter, high-frequency fluctuations in the density log are assumed to be instrumental noise. To remove the effect of this high-frequency noise, we low-pass filtered all logs with a length-scale cut-off of 10 cm. To assess the correlation between logs using different methods we calculated the correlation coefficient between the logs in windows of approximately 2.5 m. These "windowed" correlation coefficients are shown in Figure 6.5, and the data from each window are shown in Figure 6.6. As can be seen in Figure 6.5, the correlation is strongly positive near the surface; however it decreases and finally goes negative near the bottom of our profile (approximately 30 meters).

6.4.3 Wavelet correlation

Simple windowed correlation of the 2 datasets may fail to show some relationships between the 2 datasets if the data are non-stationary, as we would expect for annual layers, where wavenumber increases with depth due to compaction. The size of the window chosen for correlation might then have a direct impact on the type of relationships shown by the correlation. The appropriate solution might be to use a variable window size, perhaps scaling the window size with density. Since this has many potential complications, we turn to wavelet methods, which naturally acomodate non-stationary data. As an alternative method for determining the scale-dependent correlation between two datasets, we can use the correlation between wavelet coefficients at selected scales (Whitcher and others, 2000; Cornish and others, 2004).

A wavelet transform decomposes a time (or space, in our case) series into a series of wavelet coefficients which represent the "power" the original series contains for a given

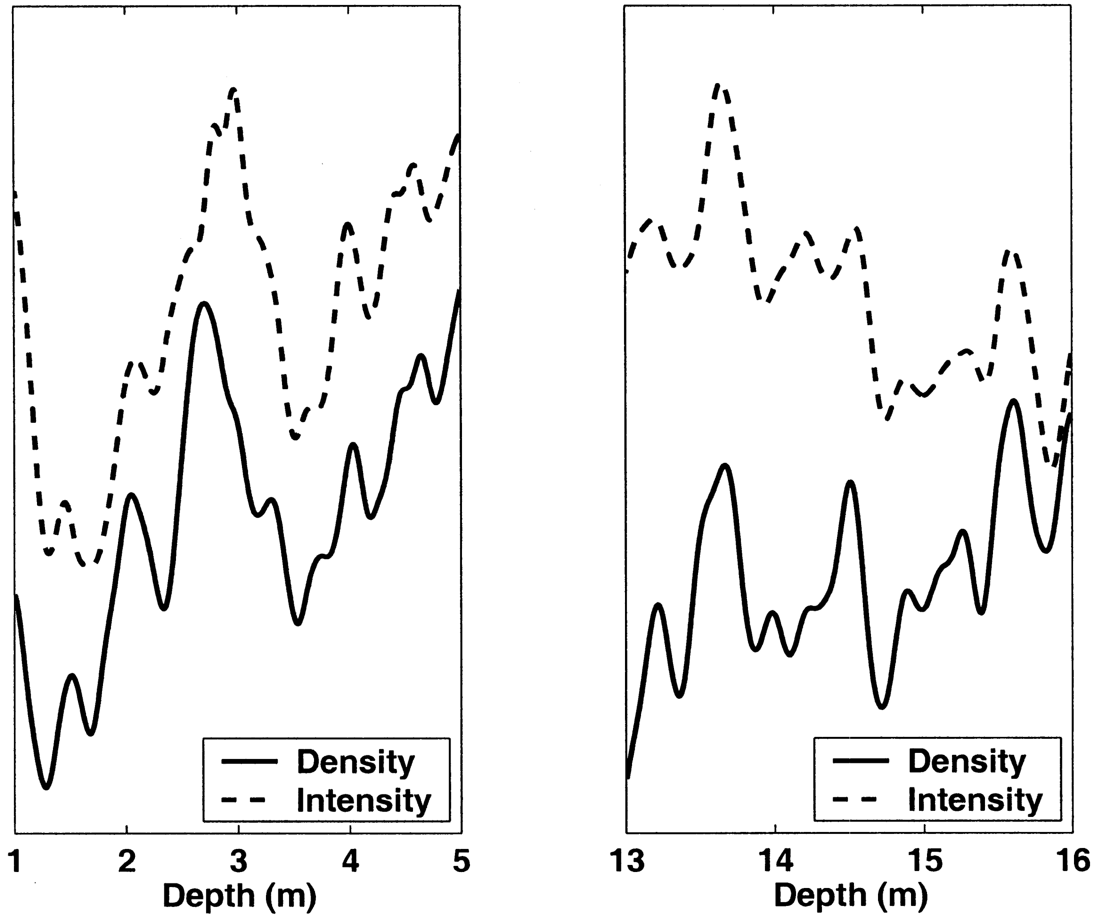

Figure 6.4: The two sets of "Landmark packets" used to co-register the 2 logs.

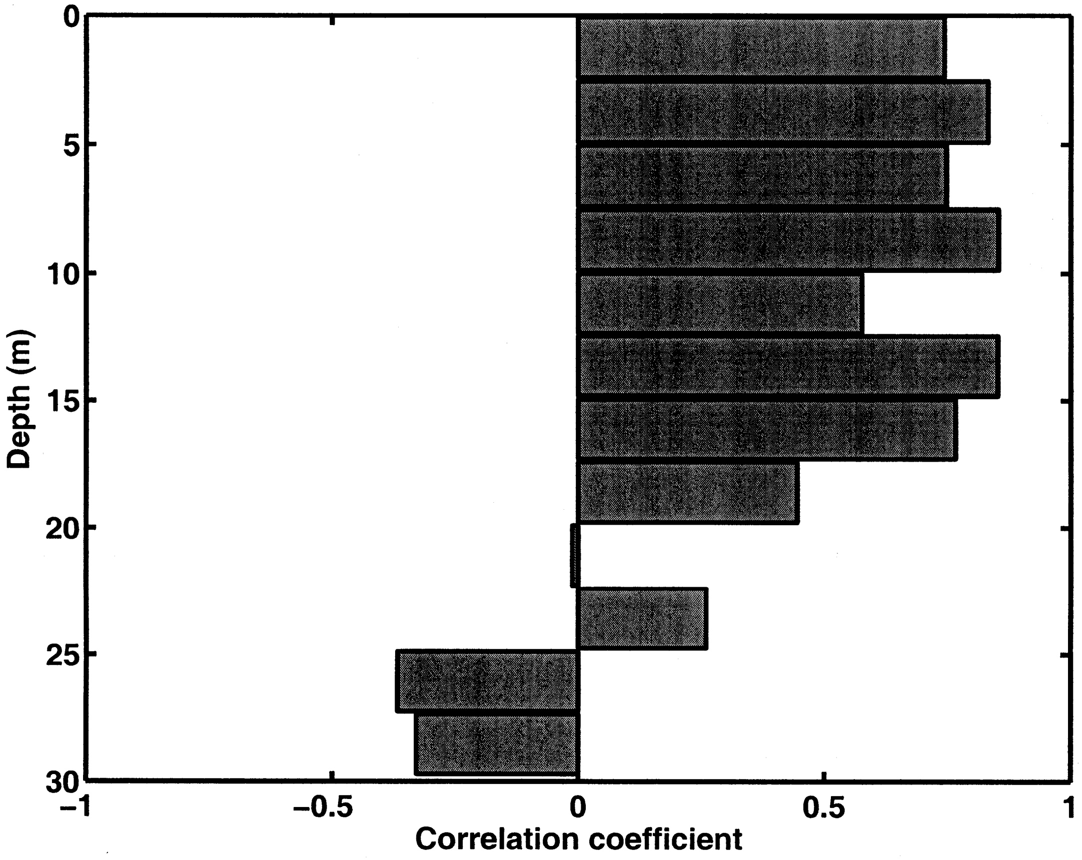

Figure 6.5: Windowed correlations between density and intensity. At shallow depths, correlation is excellent, but deeper it fades. See Discussion for details.

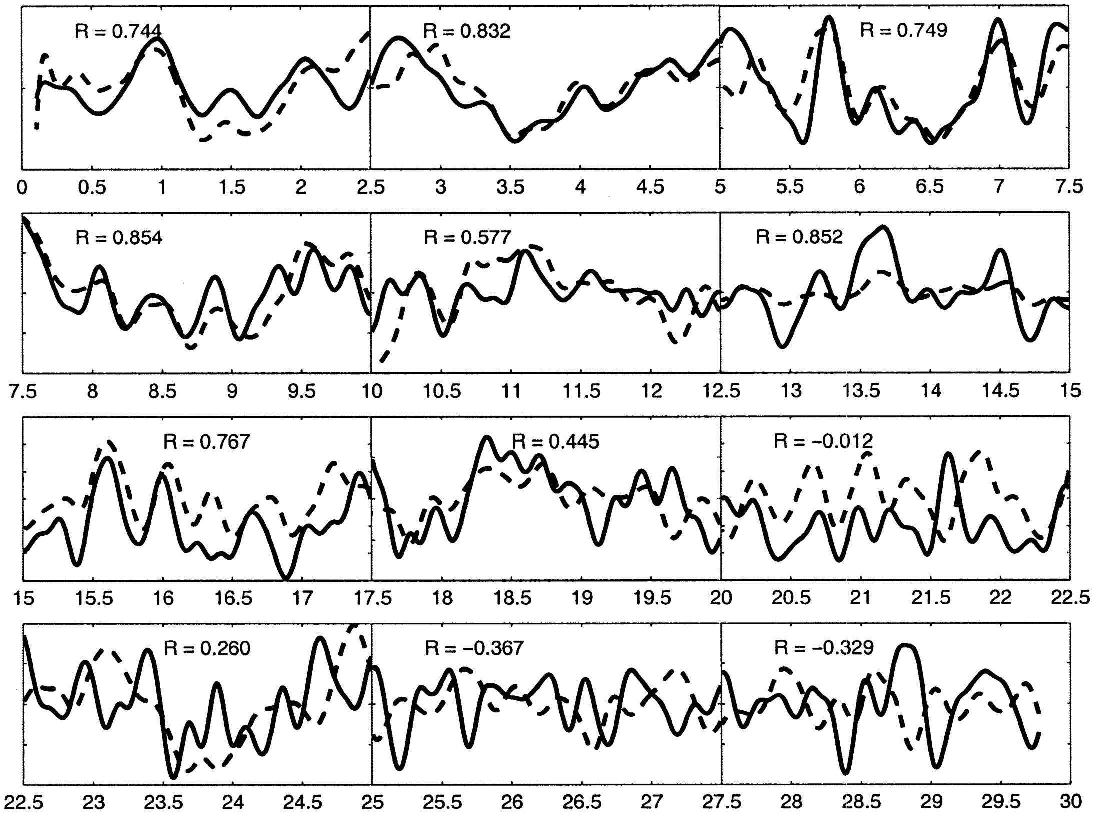

Figure 6.6: Windows for correlation. The data in each window are detrended and scaled for display. The correlation coefficient for each window is shown. Depth in meters increases along the horizontal axis.

shape and scale of the original wavelet. Correlations between the wavelet coefficients of 2 datasets at a given scale can expose or reinforce relationships that were not seen in standard filtering or Fourier analysis. We wish to determine if the "inversion of correlation" we see in the simple windowed correlation is a robust feature of the data.

Following Cornish and others (2004), we use the Maximal Overlap Discrete Wavelet Transform (MODWT) on each dataset. For each wavelet scale, we calculated the same "Windowed" correlation between the two sets of wavelet coefficients. We found the most meaningful correlations at wavelet scale 5, which corresponds to a scale of roughly 64 cm in our data. We find that at level 5, the correlation follows the same trend as our filtered data, having a positive correlation near the surface, dropping through zero to a significantly negative correlation at the bottom of the hole. Figure 6.7 shows windowed correlations at wavelet scales 3, 4, 5, and 6. Figure 6.8 shows the windows and the wavelet coefficients for level 5. The inversion of correlation can be more easily seen in the wavelet coefficients.

6.5 Discussion

As figures 6.5 through 6.8 show, we find a positive correlation between density and returned brightness in the shallow region (0-15 meters) of our survey. Also evident is that the correlation fades to near zero and becomes negative in the deeper reaches of the survey (20-30 meters). The correlation between density and brightness may point to a causal relationship between the two, or it could be indicative of the presence of another variable, such as grain size, that dominates the fluctuations of brightness yet is covariant with the density fluctuations. In this section we discuss these possibilities.

6.5.1 Density

The transformation of snow into ice is thought to take place under 3 distinct regimes with different physics contributing to compaction. In regime 1 ($\approx$ 0.3-0.55 g cm^{-3}), densification takes place primarily by grain-boundary sliding (Alley, 1987). This mechanism ceases to be dominant when the relative density of snow approaches that of random-close-packed spheres; that is, all of the ice grains have moved to the point that they are supported on all

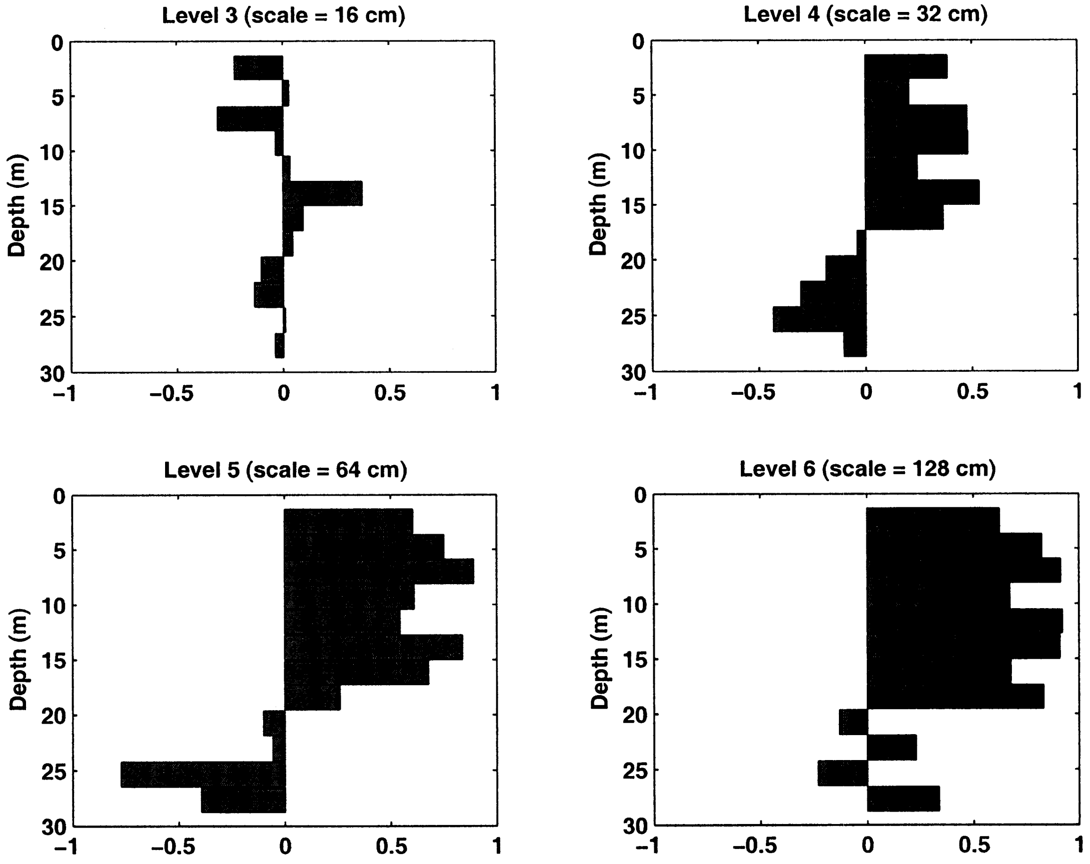

Figure 6.7: Windowed correlation between wavelet coefficients at 4 different scales. Below level 4, we see no real pattern in correlation. At levels 4 through 6 we see a pattern of decreasing correlation with depth, becoming significantly negative at levels 4 and 5. This increases our confidence in the trend of the correlation.

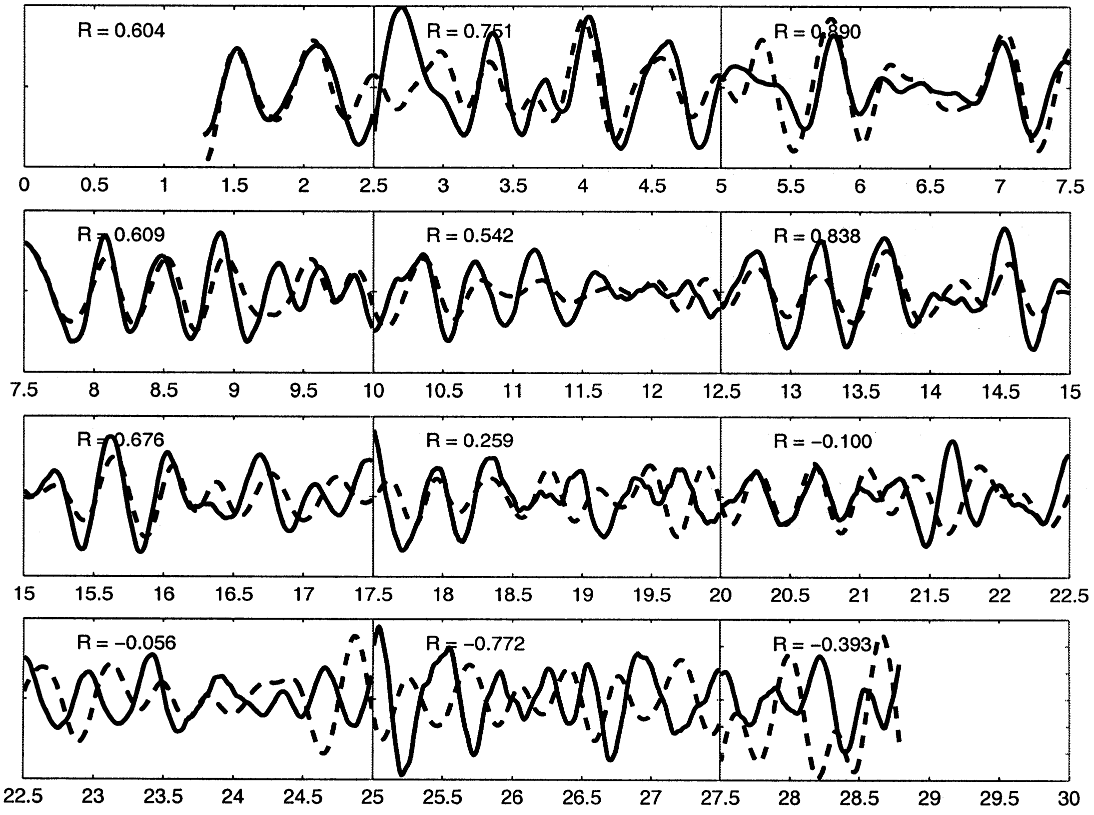

Figure 6.8: Windows for wavelet correlations at scale 5. Wavelet coefficients for the BOS log are shown as dashed lines, and coefficients for the density log are shown as solid lines. The correlation coefficient for each window is shown. Depth in meters increases along the horizontal axis. The top and bottom of the series is truncated to eliminate end-effects.

sides by other ice grains. In regime 2 ($\approx$ 0.55-0.8 g cm^{-3}) further densification then takes place by pressure sintering, in which the contact bonds between grains thicken and the interstices between the grains become smaller (Arthern and Wingham, 1998). Eventually, the interstices become isolated from one another; this transition is known as "pore close-off". In regime 3 ($\approx$ 0.8-0.92 g cm^{-3}) the confining pressure is resisted by bubble pressure in the sealed air bubbles.

In snow, firn, or ice, the amount of light returned to the borehole camera is dominated by the amount of scattering in the material. At visible wavelengths, absorption is minimal. To first order, scattering is determined by the cross-sectional area of scatterers. In the shallow regions we are concerned with here, the primary scatterer of photons is the interface between air and ice. When there is more air-ice interface surface area per unit volume, there will be more scattering.

In regime 1, densification takes place primarily by grain-boundary sliding. If no changes in grain shape occur, this process will bring more scattering surface area into a unit volume as density increases, resulting in more scattering and greater returned brightness in the borehole log. In regime 2, further densification is by pressure sintering, which involves thickening the necks between grains and producing more rounded shapes. This process is partially driven by surface energy effects and destroys surface area, so as the firn gets denser in regime 2, there is less scattering surface area per unit volume, which decreases the returned brightness in the video log.

6.5.2 Grain size and shape

Grain size and shape play an important role in scattering at visible wavelengths. At a constant density a smaller grain size results in more scattering surface area, and thus a greater backscattered intensity. Larger grain size has the opposite effect. Grain shape also has an effect on scattering surface area; a sphere is the solid shape with the lowest surface-volume ratio, so as grains become more spherical they lose scattering surface area and scattering decreases. As snow grains age, in the absence of strong thermal gradients, equitemperature metamorphism causes grains to evolve into simpler, more spherical shapes.

Several modeling studies (Bohren and Barkstrom, 1974; Wiscombe and Warren, 1980; Warren, 1982) have shown the effect of grain size, so we expect that returned brightness is indicative of grain size. Two important complications prevent us from attempting a simple correlation study between grain size and returned brightness. The most important is that grain shape in addition to grain size is very important in scattering. Grenfell and Warren (1999) showed that for any shape of snow grain, the important dimension for visible light scattering is the average path a photon takes through the grain. As an example consider a needle-shaped grain in a field of photons coming from random directions. Many more photons will pass through the grain perpendicular (or close to perpendicular) to the long axis than parallel to the long axis. Thus the best way to represent an irregularly shaped grain for scattering is as a collection of spheres with the same volume and surface area as the original grain. The second, and related, important complication arises from the reporting of grain size. When a field worker measures grain size in a snow pit or on an ice core, often the larger axis of the grain is measured rather than the shorter axis, as this often provides more information about metamorphism. For example with depth-hoar "plate-like" grains, the thickness of such a grain is the important dimension for scattering, while the diameter of the grain is likely to be reported. In this case we would predict less scattering than we would likely observe.

6.5.3 Other factors

Grain size-density correlation

Bohren and Beschta (1979) noted that, since grain size and density are often covariant, it is difficult to distinguish their contributions to radiative transfer. In the surface layers at Summit, high density fine-grained winter snow alternates with low density, large-grained summer surface hoar. Since both increasing density and decreasing grain size should lead to increasing returned brightness, the correlation between density and grain size reinforces or could be the cause of the apparent correlation between optical brightness and density. If this is the case, there must be some other explanation for the correlation trend we see deeper in the hole.

Density "inversion"

Gerland and others (1999) noted that variations in the density of a core collected at Berkner Island, Antarctica appeared to undergo an"inversion of correlation" with electrical conductivity (ECM) measurements on the core. Above 25 meters, the peaks in density were anti-correlated with peaks in ECM, the expected result since high ECM readings correspond with summer snow. However, deeper in the firn, below 25 meters, the density peaks were correlated with peaks in ECM. Gerland and others (1999) suggested that snow of an initially lower density could have a greater ability to densify than snow of an initially higher density, and thus might compress to a higher density than the layers that were initially more dense. The physics behind this suggestion are unclear. Li and Zwally (2002) modeled the densification of polar firn using a seasonal temperature cycle and found that snow deposited in late spring and summer reached higher densities than snow deposited in late fall and winter, but the difference in density in their result appears after the first few months of densification and persists as the firn is buried deeper, and so does not explain the observation of Gerland and others (1999). It should be noted also that many other studies in snow pits and shallow cores (Shoji and Langway, 1989, for example) have found the reverse to be true; higher densities correspond with winter signals in the isotope record even deeper in the core. Chemical analysis of another core from our site is planned, so we should be able to assess the possibility of this "density inversion" occurring at our site by using chemically identified summer and winter horizons.

Cable stretch

If density and returned brightness were positively correlated through the entire depth of our survey, and if some part of our depth calibration from section 6.4.1 was incorrectly calculated or if one cable stretched during the experiment, we would see a similar pattern in correlation, assuming regular oscillations; strong positive correlation near the surface, decreasing to zero and finally becoming strongly negative. If we went deep enough, or if the stretch was great enough, the correlation would become positive again. The length scale of features for which we see the strongest correlation and anti-correlation are on the order of 15-25 cm, so a differential stretch of 7-12 cm or approximately 0.2-0.5%could produce this result. Since the two measurements were indeed made with different depth-recording systems, we cannot with confidence reject the possibility that a spurious error in the depth measurement or calibration has caused this interesting correlation profile. If cable stretch or an error in calibration has caused this, we should be able to recover the original correlation by correcting the error. Both cable stretch and calibration errors would manifest themselves in a linear way; by varying our linear multiplier in section 6.4.1 we should be able to test and see if we return to an all-positive correlation with another multiplier. In figure 6.9 we have varied the linear multiplier m from equation 6.1 by 1% on each side of our preferred value from section 6.4.1. Note that the decrease in correlation with depth appears to be a robust result. Although at higher values of m the correlation stays positive and grows more positive deeper in the hole, the overall correlation is not as strong. The strongest overall correlations are seen at and near our preferred value of m. Thus we believe we are not suffering from a stretching cable or spurious calibration problem.

6.6 Conclusions and Future Work

We have measured coregistered, high-resolution, in-situ profiles of density and optical brightness at Summit. The correlation between the two logs is high at shallow depths and decreases with depth, becoming negative near the bottom of our borehole at 30 meters. With the information we have, we cannot determine uniquely the relationship between returned brightness, density, and grain size, but we believe that the change to negative correlation arises at the transition between grain-boundary-sliding and pressure-sintering as the dominant firn densification mechanism.

There are several steps that we can take to further our understanding of this process. A deeper survey would allow us to determine if the negative correlation observed near the bottom of the hole is significant. A laboratory study will also help to shed light on this issue, by measuring density, grain size, and returned brightness on firn cores. In addition, changing the geometry of the sensor by moving the light source from its current location, next to the sensor, to a different location such as far from the sensor shining towards it,

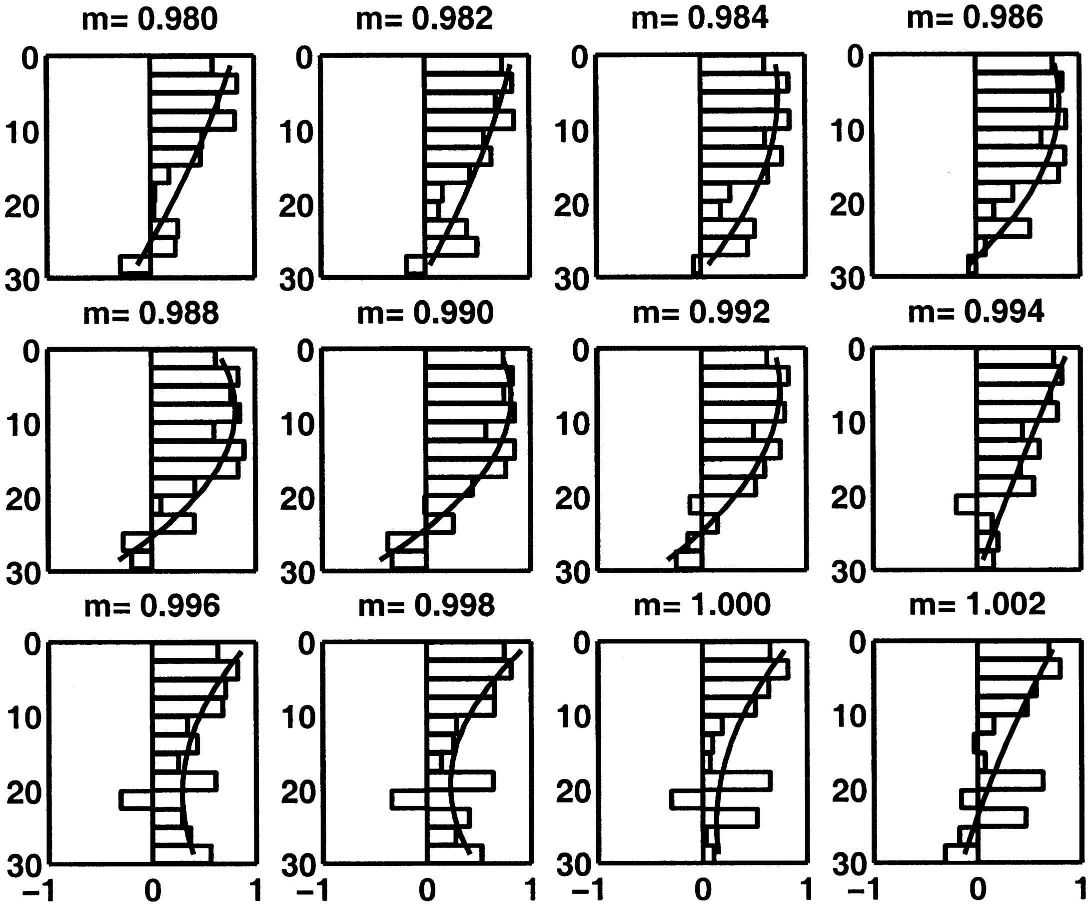

Figure 6.9: Windowed correlations under scenarios of differing cable stretch. We span our preferred m value of 0.99 and calculate the correlations if the cable were stretching or contracting. Note that the reduction in correlation with depth is a robust feature of the data.

might help in constraining the geometry for a modeling study.

Chapter 7

CONCLUSIONS AND FUTURE WORK

In this dissertation I have investigated paleoclimate and firn processes via an in-situ approach of borehole logging. In this chapter, I summarize the major findings of each chapter, under 2 broad categories. I also suggest directions for future work in improving the measurements and analysis.

7.1 Measuring vertical strain

Chapters 2 through 4 are concerned with measuring vertical strain in polar firn, at several locations in East Antarctica, West Antarctica, and Greenland.

7.1.1 New methods

In chapters 2 and 3, I presented methods of measuring vertical strain using artificial markers, detected by a video camera and also by a "tuned-coil" metal detector. These methods work well, but as stated in these chapters they both suffer the weakness of dependence on the artificial markers. At Siple Dome in particular the markers were caught by the measuring tool and displaced in the hole, complicating the analysis. In chapter 4, I introduced a method for measuring vertical strain eliminating the artificial markers and relying solely on natural variations in the returned brightness of the borehole wall. In chapters 2 and 6, I have used statistical methods (bootstrapping and wavelets, respectively) which, although useful, have seen little use in the glaciology literature.

7.1.2 Depth-age profile

To investigate paleoclimate using these vertical strain measurements, I can infer a depth-age profile from the measured vertical strain rates. Since this depth-age profile is based on direct measurement, it is an independent estimate. It is based on the assumption of steady-state, and can be compared to layer-counted ages where annual layers are resolvable to test this assumption. If the steady-state assumption is valid, the continuity model of the depth-age scale can constrain the accumulation rate.

7.1.3 Density profile

Detailed knowledge of the vertical strain profile can be found using an extension of the techniques presented in chapter 4 (see "Future work" below). Since in the firn most vertical motion is due to firn compaction and not dynamic thinning, the vertical strain profile will provide us with a detailed picture of how firn compaction progresses.

7.2 Properties of the borehole wall

The second broad category of information that can be obtained using Borhole Optical Stratigraphy is information that can be gleaned from a single log of a borehole. In this case, we are not concerned with tracking features, but rather we are concerned with what the features actually are.

7.2.1 Annual layers

In chapter 5, I showed that we can resolve annual layers in polar firn, at least at the Siple Dome site. This follows from the same assumptions that come out of ice core visual stratigraphy, mainly that summer and winter snow look different. My picks for annual layers did not "line up" exactly with those of my co-authors (Richard Alley and Ken Taylor), very likely due to spatial variability; the layers I compared to were picked on a core taken 50 meters away from my logging site.

7.2.2 Density

In chapter 6 I presented the results of an experiment in which my co-author, Liz Morris, logged density using a neutron-scattering device in a borehole which I had logged using

BOS. Although more work is needed to establish a BOS measurement of density, there is clearly a density signal in the optical stratigraphy.

7.3 Future work

More can be learned from these in-situ experiments. Advances in technique and in analysis will hopefully allow an even better understanding of past climate and firn processes.

7.3.1 Vertical strain

In an experiment currently underway at Summit, Greenland, we are measuring vertical strain in the firn in greater spatial and temporal detail than it has been measured in the past. To increase temporal detail, we have taken advantage of the winter-over presence at Summit to have the science technicians make measurements on a monthly basis. This will allow us to asses the possibility that firn densification has a seasonal cycle associated with the thermal regime. In addition to temporal detail, we've also increased the spatial detail we are measuring. We have increased the horizontal spatial detail as well by measuring an array of four holes at summit. To increase the vertical resolution of our technique, more advanced analysis is needed. A promising technique based on wavelet analysis (eg. Percival and Walden, 2000) uses the continuous wavelet transform to identify common landmarks in a pair of curves, and generates a warping function from one curve to the other (Bigot, 2003). The original intent is for co-registering curves based on landmarks, and its application to vertical strain is in identifying the warping function- this is our strain profile. This will allow us to get much greater detail in the strain rate profile.

7.3.2 Properties of the firn

The next step in understanding the interaction between light and firn is in the laboratory. I have planned a project that will do just this- study ice cores in the laboratory using our video camera. At the National Ice Core Laboratory, with access to many of the world's cores, we will conduct a "ground-truthing" experiment, in which we compare returned light intensity with datasets taken by other investigators of such things as density, grain size, chemistry, aerosols, and any other datasets we can obtain. In addition to this empirical comparison, we will also conduct radiative-transfer modeling experiments. Although we can see much with these techniques, I believe there is still much more to be seen.

BIBLIOGRAPHY

Alley, R. B. 1987. Firn densification by grain-boundary sliding: a first model. *Journal de Physique*, **3**(48), 249–256.

Alley, R. B. 1988. Concerning the deposition and diagenesis of strata in polar firn. *Journal of Glaciology*, **34**(118), 283–290.

Alley, R. B. and G. A. Woods. 1996. Impurity influence on normal grain growth in the GISP2 ice core, Greenland. *Journal of Glaciology*, **42**(141), 255 – 260.

Alley, R. B. and others. 1997. Visual-stratigraphic dating of the GISP2 ice core: basis, reproducibility, and application. *Journal of Geophysical Research*, **102**(C12), 26,367–26,381.

Arthern, R. J. and D. J. Wingham. 1998. The natural fluctuations of firn densification and their effect on the geodetic determination of ice sheet mass balance. *Climatic Change*, **40**, 605–624.

Bay, R. C., N. Bramall and P. B. Price. 2003. Ice logging with light and sound. *EOS, Trans. American Geophysical Union*, **84**(9).

Bigot, J. 2003. Landmark-based registration of 1d curves and functional analysis of variance with wavelets. Technical Report 0333, IAP Statistics Network.

Bohren, C. F. and B. R. Barkstrom. 1974. Theory of the optical properties of snow. *Journal of Geophysical Research*, **79**, 4527–4535.

Bohren, C. F. and R. L. Beschta. 1979. Snowpack albedo and snow density. *Cold Regions Science and Technology*, **1**, 47–50.

Cornish, C. R., C. S. Bretherton and D. B. Percival. 2004. Wavelet analysis of marine atmospheric boundary layer turbulence during epic. *Journal of Climate- Submitted.*

Drewry, D. J. 1982. Ice flow, bedrock, and geothermal studies from radio-echo sounding inland of McMurdo Sound, Antarctica. *In* C. Craddock, *ed*, *Antarctic Geoscience*. University of Wisconsin Press, 977–983.

Dunbar, N., G. Zielinski and D. Voisins. 2003. Tephra layers in the Siple Dome and Taylor Dome ice cores, Antarctica: Sources and correlations. *Journal of Geophysical Research*, **108**(B8). doi:10.1029/2002JB002056.

Elsberg, D. H., W. D. Harrison, E. Husmann, J. Morack, E. C. Pettit, E. D. Waddington and M. A. Zumberge. 2004. Strain rates and short term strain events measured at Siple Dome, Antarctica. *Journal of Glaciology*. in review.

Fitzpatrick, J. J. 1994. Preliminary report on the physical and stratigraphic properties of the Taylor Dome ice core. *Antarctic Journal of the U.S.*, **29**(5), 84–86.

Gerland, S., H. Oerter, J. Kipfstuhl, F. Wilhelms, H. Miller and W. D. Miners. 1999. Density log of a 181 m long ice core from Berkner Island, Antarctica. *Annals of Glaciology*, **29**, 215 – 219.

Grenfell, T. C. and S. G. Warren. 1999. Representation of a nonspherical ice particle by a collection of independent spheres for scattering and absorption of radiation. *Journal of Geophysical Research*, **104**(D24), 31697–31709.

Grootes, P. M., E. J. Steig and C. Massey. 1991. "Taylor Ice-Dome" study: Reconnaissance 1990-1991. *Antarctic Journal of the U.S.*, **26**(5), 69–72.

Grootes, P. M., E. J. Steig and M. Stuiver. 1994. Taylor Ice Dome study 1993-1994: An ice core to bedrock. *Antarctic Journal of the U.S.*, **26**(5), 79–81.

Grootes, P. M., E. J. Steig, M. Stuiver, E. D. Waddington, D. L. Morse and M.-J. Nadeau. 2001. The Taylor Dome study Antarctic ^{18}o record and globally synchronous changes in climate. *Quaternary Research*, **56**, 289–298.

Hamilton, G. S. 2002. Mass balance and accumulation rate across Siple Dome, West Antarctica. *Annals of Glaciology*, **35**, 102–106.

Hamilton, G. S. and I. M. Whillans. 1996. Global positioning system measurements of ice-sheet mass balance using the "coffee-can" method. *Antarctic Journal of the U.S.*, **31**(2), 86–88.

Hamilton, G. S., I. M. Whillans and P. J. Morgan. 1998. First point measurements of ice-sheet thickness change in Antarctica. *Annals of Glaciology*, **27**, 125–129.

Hawley, R. L. and E. D. Waddington. 2005. Vertical strain measurements in firn using Borehole Optical Stratigraphy. *Journal of Glaciology*, **1**(1), 1–2. in prep.

Hawley, R. L., E. D. Waddington, D. L. Morse, N. W. Dunbar and G. A. Zielinski. 2002. Dating firn cores by vertical strain measurements. *Journal of Glaciology*, **48**(162), 401 – 406.

Hawley, R. L., E. D. Waddington, R. B. Alley and K. C. Taylor. 2003. Annual layers in polar firn detected by Borehole Optical Stratigraphy. *Geophysical Research Letters*, **30**(15). doi:10.1029/2003GL017675.

Hawley, R. L., E. D. Waddington, G. W. Lamorey and K. C. Taylor. 2005. Vertical-strain measurements in firn at Siple Dome, Antarctica. *Journal of Glaciology*, **1**(1), 1–2. in press.

Houghton, J. and others. 2001. *Climate Change 2001. The Scientific basis.* Cambridge University Press, Cambridge, UK.

Li, J. and H. J. Zwally. 2002. Modeled seasonal variations in firn density induced by steady-state surface air-temperature cycle. *Annals of Glaciology*, **34**, 299–302.

Meese, D., A. Gow, R. Alley, G. Zielinski, M. Ram, K. Taylor, P. Mayewski and J. Bolzan. 1997. The greenland ice sheet project 2 depth-age scale: Methods and results. *Journal of Geophysical Research*, **102**(c12), 26,411 – 26,423.

Meese, D. A., A. J. Gow, P. M. Grootes, P. A. Mayewski, M. Ram, M. Stuiver, K. C. Taylor, E. D. Waddington and G. Zielinski. 1994. The accumulation record from the GISP2 core as an indicator of climate change throughout the holocene. *Science*, **266**, 1680–1682.

Morris, E. M. and J. D. Cooper. 2003. Density measurements in ice boreholes using neutron scattering. *Journal of Glaciology*, **49**(167), 599–604.

Morse, D. 1997. *Glacier Geophysics at Taylor Dome, Antarctica.* (Ph.D. thesis, University of Washington.)

Morse, D. L. and E. D. Waddington. 1992. Glacier geophysical studies for an ice core site at Taylor Dome: year two. *Antarctic Journal of the U.S.*, **27**(5), 59–61.

Morse, D. L. and E. D. Waddington. 1993. Glacier geophysical studies at Taylor Dome: year three. *Antarctic Journal of the U.S.*, **28**(5), 67–69.

Morse, D. L., E. D. Waddington and E. J. Steig. 1998. Ice age storm trajectories inferred from radar stratigraphy at Taylor Dome, Antarctica. *Geophysical Research Letters*, **25**(17), 3383–3386.

Morse, D. L., E. D. Waddington, H. P. Marshall, T. A. Neumann, E. J. Steig, J. E. Dibb, D. P. Winebrenner and R. J. Arthern. 1999. Accumulation rate measurements at Taylor Dome, East Antarctica: Techniques and strategies for mass balance measurements in polar environments. *Geografiska Annaler*, **81**(4), 683–694.

Nereson, N. A. 1998. *The flow history of Siple Dome and Ice Streams C and D, West Antarctica: inferences from geophysical measurements and ice flow models.* (Ph.D. thesis, University of Washington.)

Paterson, W. S. B. 1994. *The physics of glaciers.* Pergamon Press, Oxford, 3rd edition.

Paterson, W. S. B., R. M. Koerner, D. Fisher, S. J. Johnsen, H. B. Clausen, W. Dansgaard, P. Bucher and H. Oeschger. 1977. An oxygen-isotope climatic record from the Devon Island ice cap, arctic Canada. *Nature*, **266**, 508–511.

Percival, D. B. and A. T. Walden. 2000. *Wavelet methods for time series analysis.* Cambridge University Press, Cambridge, UK.

Picciotto, E. A. and S. Wilgain. 1963. Fission products in Antarctic snow, a reference level for measuring accumulation. *Journal of Geophysical Research*, **68**(21), 979–987.

Press, W. H., B. P. Flannery, S. A. Teukolsky and W. T. Vetterling. 1992. *Numerical Recipes in C, The Art of Scientific Computing - Second Edition.* Cambridge Univerity Press, Cambridge, England.

Ram, M. and B. G. Koening. 1997. Continuous dust concentration profile of pre-holocene ice from the greenland ice sheet project 2 ice core: Dust stadials, interstadials, and the eemian. *JGR*, **102**(c12), 26,641 – 26,648.

Raymond, C. F., J. Rogers, P. Taylor and B. Koci. 1994. Vertical strain measurement in core holes. *Mem. Nat'l Inst. Polar Res.*, **49**, 234–240. Special Issue.

Raymond, C. F., B. Weertman, L. Thompson, E. Mosley-Thompson, D. Peel and R. Mulvaney. 1996. Geometry, motion and mass balance of Dyer Plateau, Antarctica. *Journal of Glaciology*, **42**(142), 510–518.

Rogers, J. C. and E. R. LaChapelle. 1974. The measurement of vertical strain in glacier bore holes. *Journal of Glaciology*, **13**(68), 315–319.

Scambos, T. A., M. J. Dutkiewicz, J. C. Wilson and R. A. Bindschadler. 1992. Application of image cross-correlation to the measurement of glacier velocity using satellite image data. *Remote Sens. Environ.*, **42**, 177–186.

Shoji, H. and C. Langway. 1989. Physical property reference horizons. *In The environmental record in Glaciers and Ice Sheets.* John Wiley & Sons Limited, 161–175.

Spencer, M. K., R. B. Alley and T. T. Creyts. 2001. Preliminary firn-densification model wtih 38-site dataset. *Journal of Glaciology*, **47**(159), 671–676.

Steig, E. J., D. L. Morse, E. D. Waddington and P. J. Polissar. 1998. Using the sunspot cycle to date ice cores. *Geophysical Research Letters*, **25**, 163–166.

Steig, E. J., D. L. Morse, E. D. Waddington, M. Stuiver, P. Mayewski, S. Whitlow and M. Twickler. 2000. Wisconsinan and Holocene climate history from an ice core at Taylor Dome, western Ross Embayment, Antarctica. *Geografiska Annaler*, **82a**, 213–235.

Taylor, K. C., R. B. Alley and E. Brook. 2002. How to date an ice core without breaking a sweat. *Eos Trans. AGU*, **83**(47).

Taylor, K. C. and others. 2004. Dating the Siple Dome, Antarctica ice core by manual and computer interpretation of annual layering. *Journal of Glaciology*. In review.

Waddington, E. D., D. Morse, M. Balise and J. Firestone. 1991. Glacier geophysical studies for and ice core site at "Taylor Dome". *Antarctic Journal of the U.S.*, 71–73.

Waddington, E. D., D. Morse, P. Grootes and E. Steig. 1993. The connection between ice dynamics and paleoclimate from ice cores: A study of Taylor Dome, Antarctica. *In* W. R. Peltier, *ed*, *Ice in the Climate System*, volume I 12 of *NATO ASI Series I*. Springer-Verlag, 499–516.

Waddington, E. D., D. L. Morse and G. Clow. 1994. Glacier geophysics at Taylor Dome: Year 4. *Antarctic Journal of the U.S.*, **29**(5), 82–83.

Warren, S. 1982. Optical properties of snow. *Reviews of Geophysics and Space Physics*, **20**(1), 67–89.

Whitcher, B., P. Guttorp and D. B. Percival. 2000. Wavelet analysis of covariance with application to atmospheric time series. *Journal of Geophysical Research*, **105**(D11), 14,191–14,962.

Wiscombe, W. J. and S. G. Warren. 1980. A model for the spectral albedo of snow, i, pure snow. *Journal of Atmospheric Science*, **37**, 2712–2733.

Zumberge, M. A., D. H. Elsberg, W. D. Harrison, E. Husman, J. L. Morack, E. C. Pettit and E. D. Waddington. 2002. Measurement of vertical strain and velocity at Siple Dome, Antarctica, with optical sensors. *Journal of Glaciology*, **48**(161), 217–225.

Zwally, H. and J. Li. 2002. Seasonal and interannual variations of firn densification and ice-sheet surface elevation at the greenland summit. *Journal of Glaciology*, **48**(161).

VITA

Name: Robert L. Hawley

Education:

BS Geological Sciences, University of Washington, 1997

Ph. D Geophysics, University of Washington, 2005

Dissertation title:

In-Situ Investigations of Paleoclimate and Firn Processes

Publications:

Hawley, R.L., E.D. Waddington, G.L. Lamorey, and K.C. Taylor. Vertical-strain measurements in firn at Siple Dome, Antarctica. Journal of Glaciology. in press.

Hawley, R.L., E.D. Waddington, R.B. Alley, and K.C. Taylor. 2003. Annual layers in polar firn detected by Borehole Optical Stratigraphy. Geophysical Research Letters 30(15), doi:10.1029/2003GL017675.

Hawley, R.L., E.D. Waddington, D.L. Morse, N.W. Dunbar, and G.A. Zielinski. 2002. Dating firn cores by vertical strain measurements. Journal of Glaciology, 48(162), 401 - 406.

Albert, M.R. and R.L. Hawley. 2002. Seasonal changes in surface roughness characteristics at Summit, Greenland: implications for snow and firn ventilation. Annals of Glaciology 35, 510-514.

Albert, M.R. and R.L. Hawley. 2000. Seasonal differences in surface energy exchange and accumulation at Summit, Greenland. Annals of Glaciology 31, 387-390.

Abstracts and research summaries:

Hawley, R.L., E.M. Morris, and E.D. Waddington. 2004. Borehole Optical Stratigraphy and Neutron Scattering Density measurements at Summit, Greenland. EOS, Trans. AGU, fall meeting supplement, Abstract C31B-0323.

Hawley, R.L., E.D. Waddington, J.R. McConnell, and D.P. Winebrenner. 2003. Lightweight shallow ice coring and borehole logging can provide decadal- to millenial-scale indicators of climate change around the arctic basin. SEARCH Open Science Meeting, Seattle, Washington.

Hawley, R.L., and E.D. Waddington. 2002. Borehole Optical Stratigraphy: Investigating Paleoclimate through the optical properties of ice. EOS, Trans. AGU, 83(47) fall meeting supplement, Abstract C62A-0907.

Dibb, J.E., R. Hawley, S. Sturges, P. Austin, and P. Smith. 1998. Air-snow relationships at Summit, Greenland: the 1997-98 Winter-Over Experiment. EOS, Trans. AGU, Fall meeting supplement, Abstract H12H-02.

Blake, N.J., D.R. Blake, F.S. Rowland, J.E. Dibb, B. Hawley, S. Sturges, and J.D. Kahl. 1998. Year-round measurements of atmospheric nonmethane hydrocarbons, halocarbons, and light alkyl nitrates at Summit, Greenland between June 1997 and April 1998. EOS, Trans. AGU, Fall meeting supplement, Abstract H12H-05.

Arsenault, M.A., J.E. Dibb, R. Hawley, and S. Sturges. 1998. Soluble ionic composition of snow at Summit, Greenland from the 1997-1998 winter-over. EOS, Trans. AGU, Fall meeting supplement, Abstract H12H-07.

Hawley, R., and M.R. Albert. 1998. Physical snow surface characteristics during the 1997-1998 winter-over experiment at Summit, Greenland. EOS, Trans. AGU, Fall meeting supplement, Abstract H12H-09.

Albert, M.R., and R. Hawley. 1998. Meterology and the surface energy balance during the 1997-1998 winter-over project at Summit, Greenland. EOS, Trans. AGU, Fall meeting supplement, Abstract H12H-12.

Hawley, R.L., G.D. Clow, E.D. Waddington, J. Fitzpatrick, and J. Dibb. 1997. Recent climate from physical properties of firn at Taylor Dome, Antarctica. International Symposium on Antarctica and Global Change, Hobart, Australia.